Master Thesis

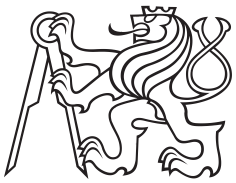

Czech Technical University in Prague

F3

Faculty of Electrical Engineering
Department of Measurement

Stabilization of eVTOL aircraft in the hovering mode using reaction wheels

Hamza Muminović

Supervisor: doc. Ing. Martin Hromčík, Ph.D
Field of study: Aerospace Engineering
Subfield: Avionics
May 2024

MASTER‘S THESIS ASSIGNMENT

I. Personal and study details

Student's name: **Muminović Hamza** Personal ID number: **516325**

Faculty / Institute: **Faculty of Electrical Engineering**

Department / Institute: **Department of Measurement**

Study program: **Aerospace Engineering**

Branch of study: **Avionics**

II. Master’s thesis details

Master’s thesis title in English:

Stabilization of eVTOL aircraft in the hovering mode using reaction wheels

Master’s thesis title in Czech:

Stabilizace eVTOL prostředků pomocí reakčních kol během vzletu a přistání

Guidelines:

Reaction wheels are mostly used for precise orientation control in satellites. The goal of this thesis is to study the potential use-cases for reaction wheels in eVTOL aircraft, namely, for roll stabilization. Using such a stabilization mechanism instead of propulsion motors could lead to faster responses and more effective disturbance attenuation. For comparison purposes simulations shall be used which will show the behavior of a eVTOL aircraft when equipped with both kinds of aforementioned stabilizing systems.
1) Develop and implement a simulation model of an eVTOL vehicle in the hovering mode, capturing flight dynamics, wind gusts, propeller characteristics, and interactions with the reaction wheel (RW) subsystem.
2) Parameterize the model according to a selected existing eVTOL project aircraft. Alternatively, use available mass and aerodynamics data related to an existing classical aircraft of similar dimensions and flight performance indicators.
3) Design two alternative hovering stabilization control laws - built on PID controllers and LQ theory respectively. Discuss their performance.
4) Compare performance of the RW-equipped eVTOL to the standard case of stabilization by propellers. Discuss settling times, overshoots, passanger comfort, with respect to wind gusts and turbulences.
5) Develop a comparison analysis of the aircraft total weight (MTOW), regarding the RW-equipped eVTOL and the standard case of stabilization by propellers. Consider datasheet parameters of existing suitable off-the-shelf components.

Bibliography / sources:

[1] Roger W. Pratt Johnson Flight Control Systems: Practical Issues in Design and Implementation. Institution of Engineering and Technology, 2000
https://app.knovel.com/kn/resources/kpFCSPIDI2/toc
[2] B. L. Stevens, F. L. Lewise. N. Johnson Aircraft Control and simulation . Third edition, John Wiley & Sons, Inc. 2016
https://ebookcentral.proquest.com/lib/cvut/reader.action?docID=4039442
[3] Franklin, James A.. (2002). Dynamics, Control, and Flying Qualities of V/STOL Aircraft. American Institute of Aeronautics and Astronautics (AIAA)
https://app.knovel.com/kn/resources/kpDCFQVST2/toc
[4] Johnson, Wayne. Rotorcraft Aeromechanics, Cambridge University Press, 2013
https://ebookcentral.proquest.com/lib/cvut/reader.action?docID=1139714

Name and workplace of master's thesis supervisor:

doc. Ing. Martin Hromčík, Ph.D. Department of Control Engineering FEE

Name and workplace of second master's thesis supervisor or consultant:

Date of master's thesis assignment: **15.02.2024** Deadline for master's thesis submission: **24.05.2024**

Assignment valid until:
by the end of summer semester 2024/2025

doc. Ing. Martin Hromčík, Ph.D. Supervisor's signature	Head of department's signature	prof. Mgr. Petr Páta, Ph.D. Dean's signature

III. Assignment receipt

The student acknowledges that the master's thesis is an individual work. The student must produce his thesis without the assistance of others, with the exception of provided consultations. Within the master's thesis, the author must state the names of consultants and include a list of references.

.	
Date of assignment receipt	Student's signature

Acknowledgements

I would obviously like to thank my supervisor, doc. Ing. Martin Hromčík, Ph.D, for guiding me through the whole process in an optimal way. Also my thanks goes to my family for making sure that I started to exist and lastly a thank you to myself for making sure I continue to exist.

Declaration

I, Hamza Muminović, hereby declare that this thesis titled "Stabilization of eVTOL aircraft in the hovering mode using reaction wheels" is my own original work, and it has not been submitted in whole or in part for any other degree or qualification at any other university or institution. All sources used in this thesis have been duly acknowledged and referenced.

In Prague, May 2024

_____

Abstract

This thesis revolves around a new approach to the roll angle stabilization of an eVTOL aircraft in hover mode. At the center of the approach is the reaction wheel, also known as momentum wheel, which is used as the control object for the stabilization of the aircraft in question.

Since reaction wheels are used primarily in the space industry for precise orientation control of spacecraft, this thesis includes an attempt to design a reaction wheel capable for stabilization in a standard atmosphere environment, which when placed in an aircraft, will be able to help with stabilization manoeuvres.

Such a design was tested in simulations against state of the art stabilization techniques giving an overview over the feasibility of this approach.

The simulations include the reaction wheel with a corresponding BLDC motor subsystem and the aircraft subsystem as two coupled subsystems, for which linear control algorithms based on PID control were implemented.

Keywords: eVTOL, Reaction wheel, Stabilization, Hover, Simulation

Supervisor: doc. Ing. Martin Hromčík, Ph.D
Department of Control Engineering FEE

Abstrakt

Tato práce se zabývá novým přístupem k stabilizaci náklonu letounu eVTOL během vzletu a přistání. Středem tohoto přístupu je reakční kolo, též známé jako momentové kolo, které slouží jako řídící prvek pro stabilizaci zkoumaného letounu.

Vzhledem k tomu, že jsou reakční kola primárně používána v kosmickém průmyslu pro přesnou orientaci kosmických lodí, tato práce zahrnuje pokus o navržení reakčního kola schopného stabilizace v prostředí standardní atmosféry, které, až bude umístěno do letadla, bude schopno pomoci s manévry stabilizace.

Takový návrh byl testován v simulacích proti nejmodernějším stabilizačním technikám, poskytujíc přehled o proveditelnosti tohoto přístupu.

Simulace zahrnují reakční kolo s odpovídajícím podsystémem BLDC motoru a podsystémem letadla jako dvě propojené podsystémy, pro které byly implementovány lineární řídící algoritmy založené na řízení PID.

Klíčová slova: eVTOL, Reakční kolo, stabilizace, Vertikální vzlet a přistání, Simulace

Překlad názvu: Stabilizace eVTOL prostředků pomocí reakčních kol během vzletu a přistání

Contents

Figures

Tables

Chapter 1

Introduction

1.1 General overview

Ever since the first mass produced helicopter design introduced in the 1940s, the idea of a vertical take-off and landing aircraft which utilizes wings for efficiency is a interesting subject in the aviation industry. The motivation for such an aircraft lies therein, that helicopters are by design not efficient in horizontal flight for the same reasons which make them good in hover mode.

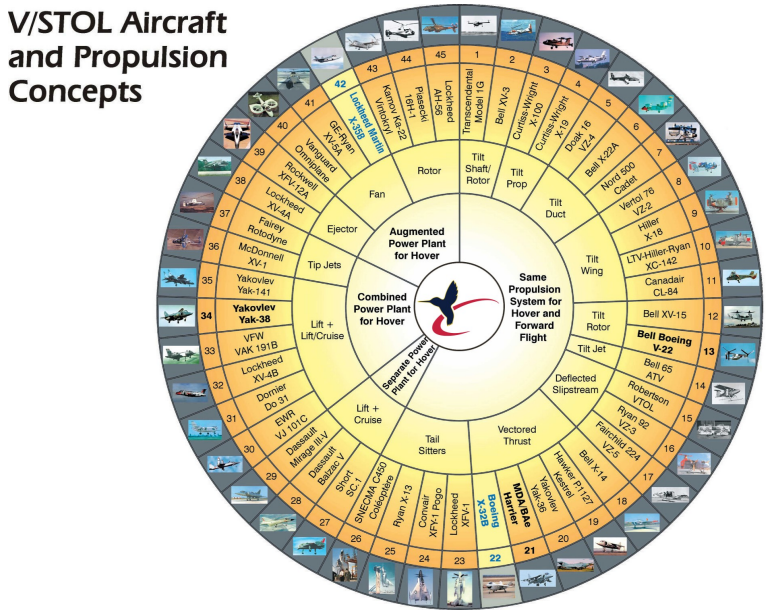

Figure 1.1: V/STOL wheel[1]

Entertainment of this idea began in the 1950s and produced many different approaches to combining the strengths of a helicopter design with the flight speed and efficiency of aircraft with wings[1]. Based on those approaches the "VTOL wheel of fortune" was created and can be seen in figure 1.1. It brings an overview over different types of V/STOL aircraft and the fundamental principle on how they overcome the barriers of hover flight. According to [1], the main problems of mechanical V/STOL aircraft, meaning non-electric

propulsion, lies in the following four points:

- Thrust generated in hover mode and in horizontal flight mode differ so much, that the propulsion systems for each needed to be either viewed as sepparate or to use far too oversized propulsion for cruise flight capabilities
- Thrust wouldn't be evenly distributed around the center of mass in hover flight
- Fuel efficiency

In the case of multiple rotor aircraft, multiple engines need to be introduced and it is known, that standard engines grow in size when the goal is the improvement of efficiency. This led to the development of fully electricaly, or hybrid, propelled VTOLs.

1.2 Electric VTOL overview

Other than the technical shortcomings of mechanical VTOLs, the motivation for electrically propelled aircraft with vertical take-off and landing capabilities lie in the ever growing need for transportation and logistics. The lack of space and the need for special infrastructure is expected to become an issue, therefore, the introduction of flying vehicles as a replacement for conventional transport vehicles is the way to go. Electric VTOLs capable of being used as personal air vehicles, air taxis or similar, is one possible solution. An example of such an aircraft is the Czech Zuri 2.0 production model, made by the Czech company *Zuri*[2], shown in figure 1.2.

Figure 1.2: Zuri 2.0 production model[2]

Electric VTOLs use brushless DC motors as drive for propellers used both for horizontal and vertical flight, overcoming the biggest issue with mechanical VTOLs, namely the difference in thrust for different flight modes. In fully electrical VTOLs the power sources are usually Li-ion batteries and hybrids use already conventional propulsion techniques as jet engines together with the batteries. The propulsion system for both modes of flight, vertical and horizontal, can be found as sepparate subsystems or as one system for both modes.

The main advantages of electrically propelled VTOLs, according to [3] and [4], are:

- Decrease in engine noise
- Reduction in overall vibration
- Improved reliability
- Improved control due to the nature of electrical systems
- Decrease in complexity relative to the mechanical approach

Similarly to electric cars, the biggest issue with electrically propelled aircraft lies in the operating range, but according to [5], there are certain misconceptions regarding the electric propulsion of aircraft, stating that $400Wh/kg$ batteries would be sufficient for acceptable operating ranges at lower costs. As a comparison, *Tesla's* 4680 lithium batteries have an energy density of $244Wh/kg$ to $296Wh/kg$.

When it comes to the stabilization of the aircraft during hover mode, the advantage of higher controlability of electric or hybrid VTOLs provides other potential techniques, not only the usual thrust vectoring or differential thrust methods. One such potential technique is entertained in this thesis, that is, using a subsystem of a reaction wheel together with a brushless DC motor capable to spin the wheel at higher speeds for the stabilization of the aircraft around one axis, analogous to spacecraft orientation control.

1.3 Reaction wheel overview

Reaction wheels in their essence are flywheels which store energy by rotating, i.e. by conserving angular momentum. As such, they found their use in the stabilization or orientation control in spacecraft by triggering momentunm exchange. A typical scheme of a reaction wheel system is shown in figure 1.3. It usually consists of the flywheel itself, an electric motor, a control system and a casing in which the whole assembly is placed. As a rule, for each rotational axis, one such assembly is integrated in the spacecraft.

Because the use of reaction wheels omits fuel use, they are found in almost every spacecraft nowadays, from small cubesats to very large satellites. NASA started using them with the *ATS-1 (Applications Technology Satellite-1)* developed in the 1960s.

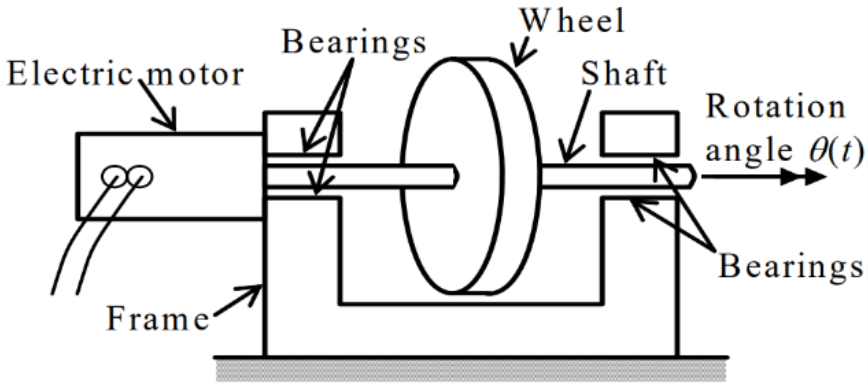

Figure 1.3: Simplified example of a reaction wheel system[6]

Spacecraft and satellites are subjected to external torques, such as solar radiation pressure or aerodynamic forces in Low Earth Orbit which can impact the orientation of the craft. The change in spacecraft angular rates because of those external torques can be measured and afterwards corrected by the reaction wheel rotation which counter-rotates the craft in the same ratio. Important to note is the fact, that the reaction wheel cannot create translational movement of the spacecraft, but only rotation[7]. This type of orientation control is extremely precise, even to the level of 0.002° error, which is one of the most important requirements in the space industry.

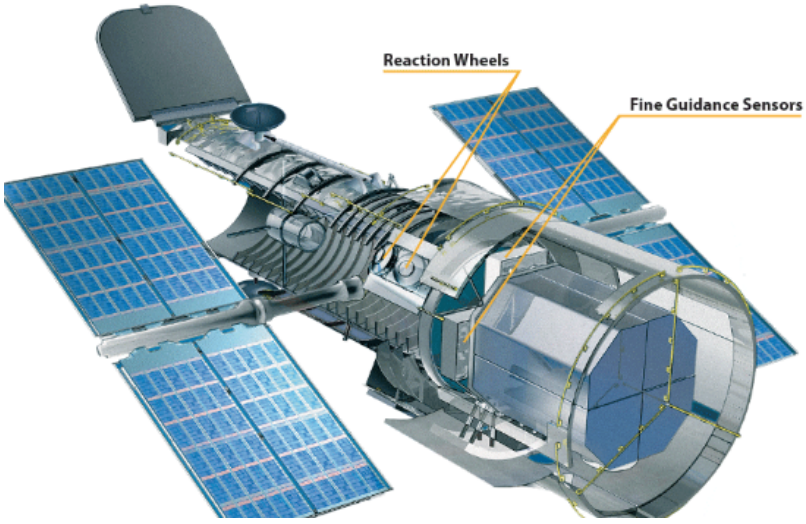

Figure 1.4: Hubble space telescope

The ability for very precise pointing control made reaction wheels usable especially for space telescopes. The Hubble Space Telescope is shown in figure 1.4 with the reaction wheel assembly pointed out. The ones used in Hubble Space Telescope are able to produce a torque of $0.8Nm$ at a maximum speed of $3000RPM$ with a rotor moment of inertia of $0.84kgm^2$ per wheel[8].

Another benefit of reaction wheels over thrusters is the longevity since there is no burning included thus material degradation is avoided, but the presence of moving parts in reaction wheels means that mechanical failures are still possible, mainly because of bearing friction which introduces wear. Other possible problems include motor failures which could be considered critical failures.

Besides the possible mechanical failures of reaction wheels, they can become saturated at the point when the rotational speed reaches its maximum. When that happens desaturation manoeuvres are necessary using thrusters.

1.4 Goals

The main motivation for this thesis is the mentioned stabilizing ability of reaction wheels, as mentioned for the case of spacecrafts. The main goal is to study the possibility of using them for the stabilization of eVTOL aircraft in hover mode instead of the usual stabilization techniques. Therefore, the following will be the main goals of this thesis:

1. Study the dynamics of eVTOL aircraft in hover mode and create an apropriate model
2. Create a general reaction wheel model
3. Analyze the impact of different materials, which can be used for the reaction wheel design, on the stabilizing ability
4. Study the possibility of reaction wheel parameter optimization for a given use case
5. Integrate the reaction wheel subsystem to the aircraft
6. Analyze the power consumption for the whole system
7. Compare the funcionality of the developed system with state-of-the-art stabilization techniques, like differential thrust stabilization

Chapter 2

Description of the system

2.1 Coordinate system

The goal here is to inspect the posibility of the use of reaction wheels for the stabilization of the roll angle of an eVTOL in hover mode, i.e. during vertical landings and take-offs. For that, it is important to define the system as a whole.

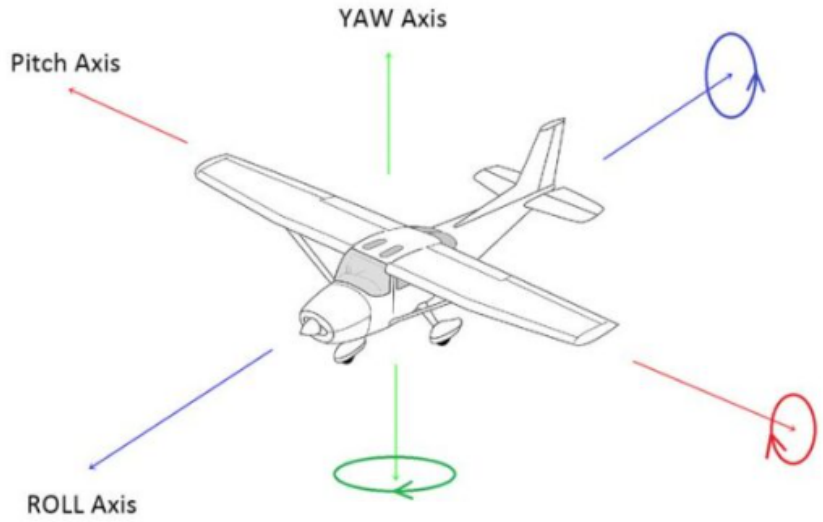

Figure 2.1: The coordinate system[9]

The aircraft is inside a coordinate system with three dimensions, namely the x axis, y axis and z axis. As shown in the figure 2.1, rotation around each of the axes is described by Euler angles. The x axis is the longitudinal axis of the aircraft and rotation around it is described by the *roll* angle (depicted by color blue on figure 2.1), the y axis is the lateral axis going from side to side of the airplane and rotation around it is described by the *pitch* angle (depicted by the color red on the same figure) and lastly, the z axis is the vertical axis of the airplane and rotation around this axis results in the *yaw* angle. In this paper, the roll dynamics will mostly be the focus.

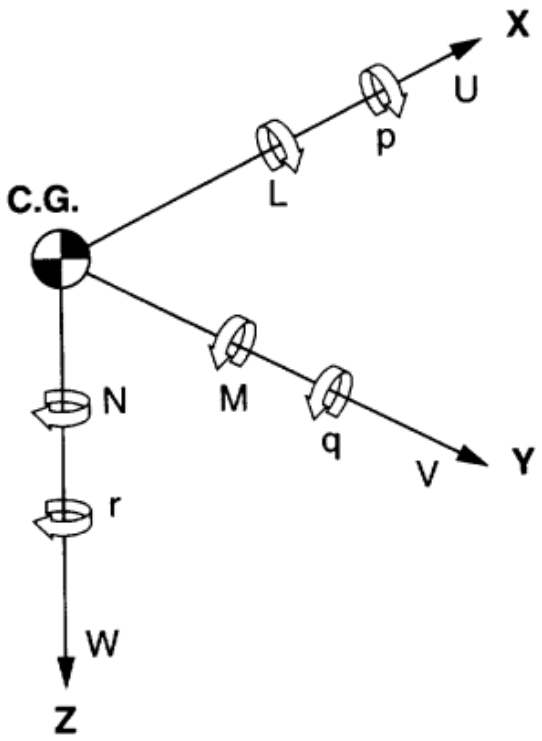

Figure 2.2: Detailed coordinate system

A more detailed free body diagram is shown in figue 2.2. The origin is placed in the center of gravity of the aircraft.

Forces along the longitudinal axis are considered to be positive when acting from the direction of the tail to the nose of the aircraft. The corresponding moments around the longitudinal axis are defined as L and the roll rate as p. The translational velocity in the longitudinal direction is described by the symbol u.

The direction of the lateral axis y is towards the right wing, thus all the forces acting in that direction on the center of gravity are considered positive. The pitching moment and pitch rate are denoted as M and q respectively. Velocity in that direction is v.

Lastly, the vertical axis z is pointing downward and all the downward pointing forces are considered positive. Rotation around the vertical axis results in yawing, therefore the yaw moments and yaw rates are denoted as N and r respectively. Downward velocity is w.

The conventions described correspond to the usual NED (North-East-Down) body reference frame.

Standard empty weight	$754kg$
Length	$8.28m$
Wingspan	$11m$
Wing area	$16.17m^2$
Moment of inertia (roll)	$2424.24kgm^2$
Moment of inertia (pitch)	$2427.3kgm^2$
Moment of inertia (yaw)	$4372.5kgm^2$

Table 2.1: Cessna 172 data

2.2 Aircraft parameters

To be able to simulate the dynamics of this system, a mathematical representation of its parts is needed. Out of the lack of publicly known and free technical information on certain real world eVTOL aircraft, mechanical parameters of a *Cessna 172* airplane will be used and it will be "imagined" as an eVTOL. It is assumed that there are two symmetrically placed electric propulsion systems on the lateral axis, on the end of each wing, which enable the aircraft to stay in hover mode.

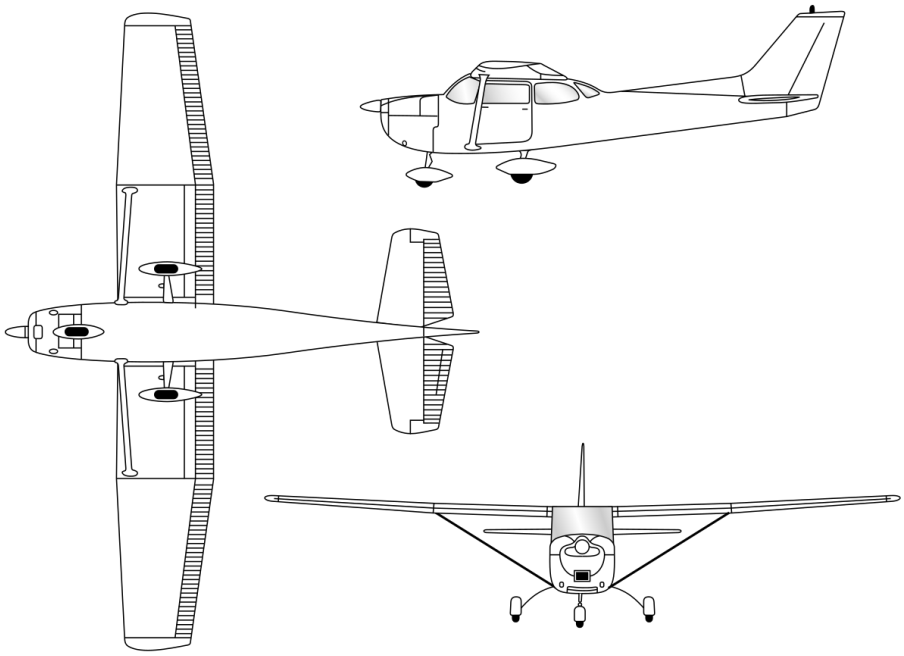

Figure 2.3: The Cessna 172 airplane

Data used[10] is shown in the table 2.1.

2.3 Reaction wheel parameters

The reaction wheel system consists of the wheel itself and a brushless DC motor which makes the rotation possible. A schematic[11] of this subsystem is shown on figure 2.4.

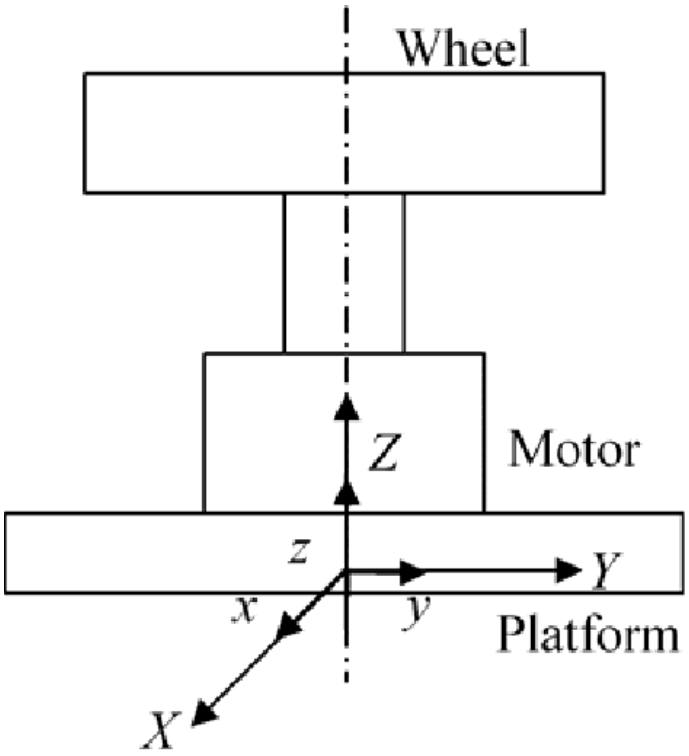

Figure 2.4: The reaction wheel schematic diagram[11]

The first assumption made is a fixed volume of the reaction wheel, i.e. the geometry is fixed and the values used correspond to some conventional reaction wheels for bigger satellites with mass ranging from $500kg$ to $1500kg$ like the Rockwell-Collins RSI series of reaction wheels. The reason for this assumption is that the analysis of which material to use is done for the same reference size for each material. The diameter of the reaction wheel is set to be $30cm$ and the height (or thickness) $7cm$. Important to note is that most of the mass in concentrated on the outer part of the wheel, therefore the mass of the inner part of the disk is much smaller than the mass of the outer part and as such will be neglected. It is also assumed, that the outer part of the wheel starts at 90% of the total radius, meaning, the whole mass of the wheel is concentrated in the outer ring which is defined by the outermost 10% of the total radius.

The reaction wheel works on the principle of conservation of angular momentum, therefore the angular momentum of the aircraft and the angular

momentum of the reaction wheel are related by[12]:

$$\dot{L}_{aircraft} = -\dot{L}_{reactionwheel} \tag{2.1}$$

from which, by integrating, the following equation can be obtained:

$$I_{aircraft} \cdot \omega_{aircraft}(t) = -I_{rw} \cdot \omega_{rw}(t) \tag{2.2}$$

Equation 2.2 shows that the rotational speed of the aircraft is a function of the physical properties of the reaction wheel (moment of inertia) and its rotational speed. In other words, for a specific stabilization maneuver of the aircraft, the reaction wheel needs to generate a specific amount of angular momentum which is a function of its rotational speed, for an already specified geometry. Naturally, there are constraints when it comes to the rotational speed and those constraints are dependant on the materials from which the wheel is made of.

2.3.1 Materials

The material used in the outer ring of the reaction wheel impacts the maximum rotational speed the wheel can withstand to rotate on without being deformed due to centrifugal stresses. A higher maximum rotational speed means potentially higher angular momentum generation. In this case, a reaction wheel is considered to be of a higher quality based on the amount of generated angular momentum for already specified geometrical properties. The maximum angular momentum generated can be calculated from:

$$L_{max} = I_{rw}\omega_{max} \tag{2.3}$$

where I_{rw} is the moment of inertia of the reaction wheel:

$$I_{rw} = \frac{1}{2} m_{rw} \left(R_1^2 + R_2^2\right) \tag{2.4}$$

which is the moment of inertia of a ring, R_1 is the radius of the inner part of the disk and R_2 is the radius of the whole disk. The mass is defined as:

$$m_{rw} = \left(R_2^2 - R_1^2\right) \rho \pi h \tag{2.5}$$

A portion of the outer ring while rotating will be under the influence of a centrifugal stress[13] shown in the following equation:

$$\sigma = \left(\frac{3+\nu}{8}\right) \rho R^2 {\omega_{rw}}^2 \tag{2.6}$$

The amount of centrifugal stress should never exceed the yield stress σ_y which is dependent on the material. From equation 2.6 a maximum rotational speed, as a function of the type of material used, can be calculated.

$$\omega_{max} = \sqrt{\frac{8\sigma_y}{(3+\nu)\rho R^2}} \tag{2.7}$$

Equation 2.7 shows the maximum "safe" angular velocity of the reaction wheel for which deformations will not occur. For a fixed geometry, the value of ω_{max} is influenced only by the properties of the material:

- ν is the Poisson ratio of the material
- σ_y is the yield stress of the material

Therefore, three different grades of materials will be analyzed: low, medium and high grade.

Low grade material

Aluminum is the obvious choice for a lightweight and sturdy material. It has a density of aproximately $2710kgm^{-3}$ with the yielding stress of $\sigma_y = 40MPa$. Knowing this, the maximum angular velocity can be calculated from equation 2.7, where $R = R_2 = 0.1 \cdot 0.15m = 0.015m$:

$$\omega_{max} = 1225.4rads^{-1} = 11988RPM \tag{2.8}$$

The moment of inertia of the lower grade aluminum reaction wheel is calculated by combining equations 2.4 and 2.5:

$$I_{rw} = 0.1038kgm^2 \tag{2.9}$$

where the mass of the aluminum reaction wheel is $m_{rw} = 2.5477kg$. From these results and equation 2.3, it is possible to calculate the maximal angular momentum generated by a low grade reaction wheel:

$$L_{max} = I_{rw}\omega_{max} = 130.2541Nms \tag{2.10}$$

As a reference, ASTROFEIN's RW6000 reaction wheel[14] from their high line of reaction wheels for big satellites, by dimensions similar to the reaction wheel presented in this paper, is able to generate a maximal angular momentum of around $100Nms$.

Medium grade material

The medium grade zone is mostly represented by titanium alloys. For analysis purposes, the titanium alloy *Ti-6Al-4V* is chosen here. Significant properties for this alloy[15] are:

- Poisson ratio: $\nu = 0.342$
- Yield stress: $\sigma_y = 970MPa$

Using the same equations as for the low grade material section, parameters of interest can be calculated:

$$\omega_{max} = 4840.7rads^{-1} = 46225RPM \tag{2.11}$$

$$I_{rw} = 0.1692kgm^2 \tag{2.12}$$

where the mass of the titanium alloy reaction wheel is $m = 4.1553kg$. Finally, the upper limit for the angular momentum generation is:

$$L_{max} = 819.1694Nms \tag{2.13}$$

Important to notice here is, that for a 61% increase in reaction wheel mass (relative to the aluminum one), the maximal angular momentum that can be generated has increased by more than 600%. The downside is, that in reality, the maximum values should never be reached since it is not recommended for the wheel to rotate continuously at maximum RPM and a certain safety margin should be included in the design process. These theoretical values serve as a comparison between the choice of materials.

High grade material

For the highest grade materials used in production of reaction wheels iron alloys (mainly stainless steel) are used. The precise alloy that was chosen is *Nickel-Cobalt-Molybdenum maraging steel* or *maraging steel 280* which is already very popular in the aerospace industry used for rocket motor casting and landing gear[13]. Values for the Poisson ratio and yield stress are:

- Poisson ratio: $\nu = 0.3$
- Yield stress: $\sigma_y = 1980MPa$

Such a reaction wheel, for the already defined geometry, would have a moment of inertia:

$$I_{rw} = 0.3063kgm^2 \tag{2.14}$$

with a corresponding mass of $m_{rw} = 7.5210kg$. The maximum angular velocity can be, again, calculated from equation 2.7:

$$w_{max} = 5163.9778rads^{-1} = 49312RPM \tag{2.15}$$

For the calculated values of moment of inertia and maximum angular velocity, the maximum angular momentum that can be generated is:

$$L_{max} = 1581.6831Nms \tag{2.16}$$

A substantial increase in mass and, consequently, moment of inertia, can be observed, but also a substantial increase in the highest possible amount of generated angular momentum. The goal is not only to pick some material which will be able to produce the biggest amount of angular momentum, but to get the most of it in that sense while using up the least amount of power, since every reaction wheel has a corresponding motor driving the shaft. Therefore, the natural thing to do next is to analyze the necessary power that needs to be brought to the shaft on which the reaction wheel is located on.

2.3.2 Reaction wheel power analysis based on material used

To do a comparison between the mentioned types of reaction wheels with respect to the power constraints, a test maneuver is defined: the aircraft is initially at a roll angle of $\theta = 10°$ with other initial conditions equal to zero, and a simple stabilizing maneuver is wanted, i.e. the reaction wheel should stabilize the aircraft to roll angle of zero degrees in 10 seconds. During this maneuver constant angular acceleration and subsequent deceleration are assumed. Half of the total time will be spent accelerating and the other half decelerating, therefore the angular acceleration of the aircraft during the half-interval is:

$$\alpha = \frac{2\Delta\theta}{\Delta t^2} \tag{2.17}$$

where $\Delta\theta = \frac{\Delta\theta_{tot}}{2} = 5°$ and $\Delta t = \frac{\Delta t_{tot}}{2} = 5s$, therefore the angular acceleration/deceleration is $\alpha = 0.007 rads^{-2}$.

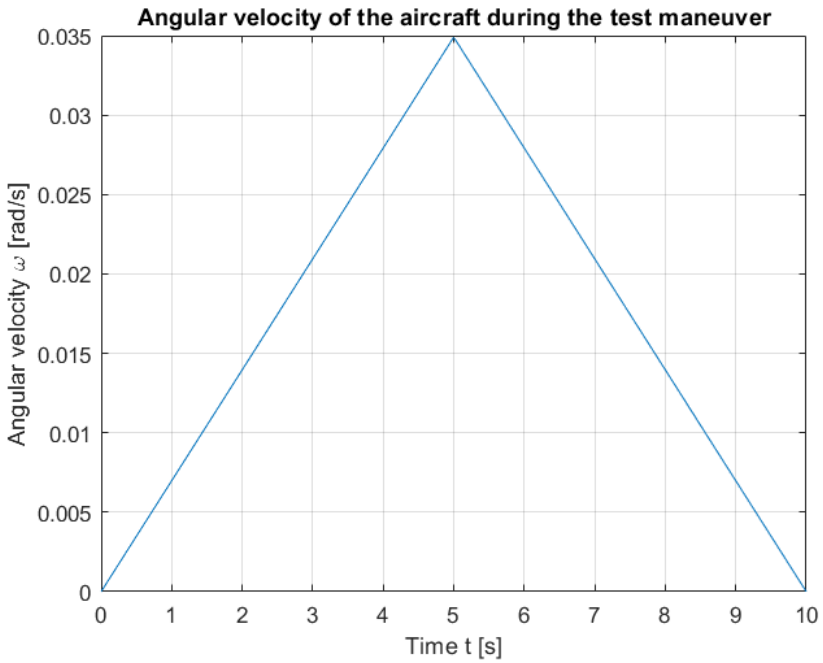

Figure 2.5: Angular velocity of the aircraft during the test maneuver

On the figure 2.5 the theoretical angular velocity of the aircraft during the maneuver is shown. The angular velocity of the aircraft is impacted only by the change in angular momentum caused by the rotation of the reaction wheel, therefore, for the minimum input power calculation only the peak value of the generated angular momentum will be considered. The point at which the generated angular momentum is at its maximum is when the aircraft reaches peak angular velocity, i.e. at timepoint $t = 5s$:

$$\omega_{max} = \alpha\Delta t \tag{2.18}$$

where $\Delta t = \frac{\Delta t_{tot}}{2} = 5s$ and $\alpha = 0.07 rads^{-2}$. Thus, the angular momentum generated is:

$$L_{aircraft} = I_{aircraft}\omega_{max} = I_{aircraft}\alpha\Delta t = 84.6205 Nms \tag{2.19}$$

The value of $I_{aircraft}$ is taken from the table 2.1, i.e. the rolling moment of inertia. According to equation 2.2 the reaction wheel at that point will have the same amount of generated angular momentum (but with a negative sign), thus it is possible to calculate the peak angular velocity of the reaction wheel:

$$\omega_{rw} = \frac{L_{aircraft}}{I_{rw}} \tag{2.20}$$

From the equation 2.20 can be seen, that the angular velocity of the reaction wheel will depend on the moment of inertia, which is depended on the material used. The mechanical power needed to be brought to the shaft is:

$$P_{mech} = \tau\omega_{rw} \tag{2.21}$$

where τ is:

$$\tau = I_{aircraft}\alpha \tag{2.22}$$

Combining equations 2.17, 2.19, 2.20, 2.21 and 2.22, the equation for minimum mechanical power necessary to be brought to the shaft of the reaction wheel for the completion of such a maneuver is:

$$P_{min} = \frac{2\omega_{rw} I_{total}\Delta\theta}{\Delta t^2} \tag{2.23}$$

where ω_{rw} is the maximum angular velocity of the reaction wheel during the maneuver, I_{total} is the moment of inertia of the whole system, $\Delta\theta$ is the total angular displacement during the time interval Δt. In this case half of the total time interval is spent accelerating and the other half decelerating. By assuming constant values of angular acceleration/deceleration, for the full maneuver the required power will be for $\Delta\theta = \frac{\Delta\theta_{tot}}{2}$ and $\Delta t = \frac{\Delta t_{tot}}{2}$ and multiplied by two because it is assumed that the same energy is required for acceleration and deceleration. Putting all of that together, the following equation is obtained:

$$P_{min} = \frac{8\omega_{rw} I_{total}\Delta\theta_{tot}}{{\Delta t_{tot}}^2} \tag{2.24}$$

For this test maneuver the values will be $I_{total} = 2424 kgm^2$, $\Delta\theta_{tot} = 10°$ and $\Delta t_{tot} = 10s$ and the parameter ω_{rw} will be dependent on the performance grade of the material.

Now, depending on the material, reaction wheels will need to rotate on different speeds to generate the required angular momentum. The dependancy of the generated angular momentum on angular velocity for the already mentioned grades of material quality is shown on figure 2.6. It is noticeable that for higher peformance grades, the shaft on which the reaction wheel is, needs to rotate at a lower angular velocity, therefore, from equation 2.24,

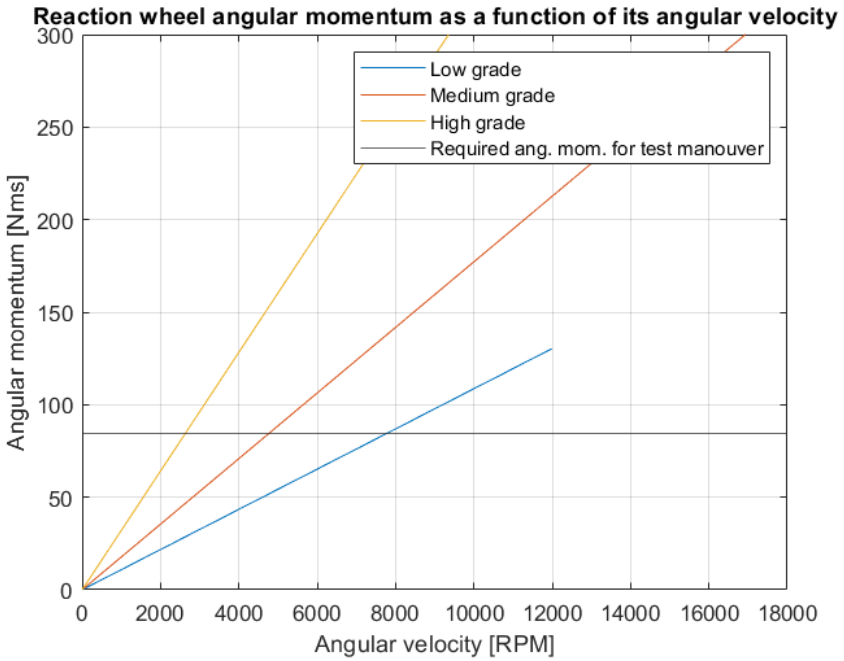

Figure 2.6: Angular momentum as a function of angular velocity for reaction wheels of different performance grades

Material	ω_{rw} [RPM]	P_{min} [kW]
Aluminum (LPG)	7788.1	27.6056
Ti-6Al-4V alloy (MPG)	4775.1	16.9256
Maraging steel 280 (HPG)	2638.2	9.3514

Table 2.2: Calculated reaction wheel parameters based on different performance grades

required mechanical power will get lower the higher the performance grade of the material is. Important to note, is that in the equation 2.24, the minimum power is indirectly correlated to the moment of inertia of the reaction wheel through the parameter ω_{rw} (which can be seen from the equation 2.20).

Using equations 2.20 and 2.24 parameters of interest were calculated for *low performance grade (LPG)*, *medium performance grade (MPG)* and *high performance grade (HPG)* reaction wheel materials for a stabilizing test maneuver from initial roll angle of 10° to 0° in 10s. Aircraft parameters were described in the previous subsection.

Comparing the minimal power which needs to be excerted by the reaction wheel DC motor, it can be concluded that the choice of material for a fixed volume reaction wheel is important, since the power requirements by going from medium performance grade to high performance grade materials are almost halved, which makes the choice of the DC motor much more flexible.

Also important to notice are the requirements for the generated angular momentum for the specified maneuver. A reaction wheel made of plain aluminum (low performance grade) is barely able to generate enough for a successful stabilization maneuver in question so it will not be considered in further analysis.

The calculated values shown in table 2.2 are calculated with many assumptions: constant acceleration/deceleration of the reaction wheel, equal time intervals for acceleration and deceleration, bearing friction is ignored and also the system is assumed to be under no disturbances. Therefore, while designing the reaction wheel subsystem a margin of *at least* 50% should be taken into consideration.

As the source of mechanical energy brought to the shaft, a brushless DC motor can be considered. The compactness and high power output of BLDC motors is of great importance, since the added mass to the aircraft should be minimal. The usual values of the efficiency factor of BLDC motors are rather high and lie between 85% and 90%, that means, that around 85% of the input electrical energy to the motor will be converted to mechanical power of the shaft on which the reaction wheel is rotating on. With all of that said, in the simulation step, a BLDC motor is an obvious choice as the power source of the reaction wheel subsystem.

Chapter 3

Mathematical model

3.1 Aircraft subsystem

The dynamics of V/STOLs and aircraft in general have been already studied to a great extent, for example, see [16] and [17]. Mathematical descriptions from said sources will be used and tailored towards the goal of this thesis.

3.1.1 Inertial forces and moments

Using the conventions and body reference frame described in previous chapters, the following equations of inertial forces and moments of the aircraft relative to body fixed axes can be writtenq[16]:

$$\sum X = m\left(\dot{U} + QW - RV\right) \tag{3.1}$$

$$\sum Y = m\left(\dot{V} + RU - PW\right) \tag{3.2}$$

$$\sum Z = m\left(\dot{W} + PV - QU\right) \tag{3.3}$$

$$\sum L = \dot{P}I_{xx} - \dot{R}I_{xz} + QR\left(I_{zz} - I_{yy}\right) - PQI_{xz} \tag{3.4}$$

$$\sum M = \dot{Q}I_{yy} + PR\left(I_{xx} - I_{zz}\right) - R^2I_{xz} + P^2I_{xz} \tag{3.5}$$

$$\sum N = \dot{R}I_{zz} - \dot{P}I_{xz} + PQ\left(I_{yy} - I_{xx}\right) + QRI_{xz} \tag{3.6}$$

where:

- m is the total mass of the aircraft
- $\sum X$ denotes the sum of inertial forces along the $x - axis$
- $\sum Y$ denotes the sum of inertial forces along the $y - axis$
- $\sum Z$ denotes the sum of inertial forces along the $z - axis$
- U is the total translational velocity along the longitudinal axis, i.e. $x - axis$
- V is the total translational velocity along the lateral axis, i.e. $y - axis$

- W is the total translational velocity along the vertical axis, i.e. $z - axis$
- P is the total roll rate
- Q is the total pitch rate
- R is the total yaw rate

The parameters denoted as I_{ik} where $i = \{x, y, z\}$ and $k = \{x, y, z\}$ are elements of the symmetrical moment of inertia tensor given by:

$$\boldsymbol{I} = \begin{bmatrix} I_{xx} & I_{xy} & I_{xz} \\ I_{yx} & I_{yy} & I_{yz} \\ I_{zx} & I_{zy} & I_{zz} \end{bmatrix} \tag{3.7}$$

The elements on the main diagonal are moments of inertia of the aircraft around the longitudinal, lateral and vertical axis, i.e. the rolling, pitching and yawing moment of inertia respectively, while the rest are named, in various sources, as moment of inertia cross products; the moment of inertia of the body in one axis relative to some other.

The equations 3.1 to 3.6 represent equations for inertial forces and moments in the body fixed NED reference frame. Important to note is that the impact of the gravitational force is not included in those equations. The gravitational force acts upon the body at all times and as such cannot be neglected. The gravitational force acts on the center of gravity, therefore it does not impact the rotation of the aircraft, that means there will be no change to equations 3.4 to 3.6.

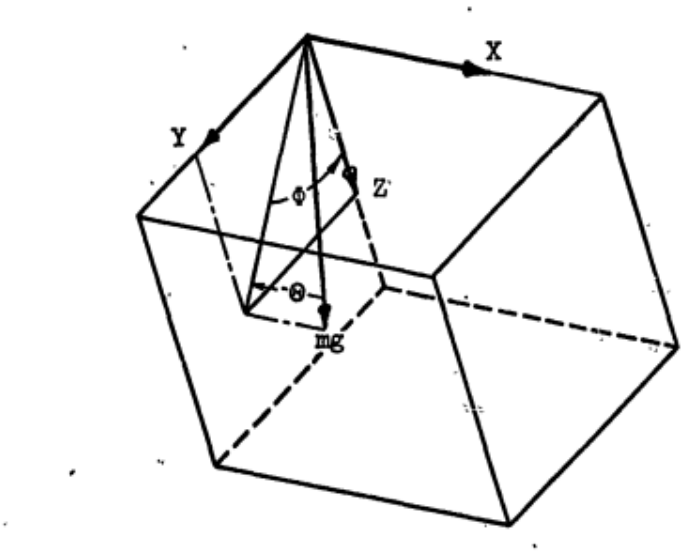

Figure 3.1: The gravitational acceleration vector in the body fixed NED reference frame[17]

Consider the figure 3.1. Creating projections of the gravitational force to each respective axis creates force increments as follows:

$$\Delta X = -mg \sin \Theta \tag{3.8}$$

$$\Delta Y = mg\cos\Theta\sin\Phi \tag{3.9}$$

$$\Delta Z = mg\cos\Theta\cos\Phi \tag{3.10}$$

Therefore, adding these to the equations 3.1 to 3.3:

$$\sum X = m\left(\dot{U} + QW - RV + g\sin\Theta\right) \tag{3.11}$$

$$\sum Y = m\left(\dot{V} + RU - PW - g\cos\Theta\sin\Phi\right) \tag{3.12}$$

$$\sum Z = m\left(\dot{W} + PV - QU - g\cos\Theta\cos\Phi\right) \tag{3.13}$$

Important to note is, that the angles Θ and Φ are not in general the pitch and roll Euler angles. They are the elevation and tilt angle respectively, meaning, angles in the context of a global inertial frame. The tilt angle is sometimes used interchangeably with Euler's roll angle but it is not always the case, especially in aviation where the tilt angle is the roll angle of the aircraft but impacted by the pitch angle. Using certain assumptions, like if we consider the flight to be horizontal above a flat Earth and at the beginning time point all the axes of both the body reference frame and the inertial frame coincide, then the elevation and tilt angle could be approximated by their corresponding Euler angles, pitch and roll (also the azimuth angle as the yaw angle).

It is possible to rewrite the equations 3.1 to 3.6 as a function of accelerations the instruments on board of the aircraft would measure. The equations are as follows:

$$X = ma_x = m\left(\dot{U} + QW - RV + g\sin\Theta\right) \tag{3.14}$$

$$Y = ma_y = m\left(\dot{V} + RU - PW - g\cos\Theta\sin\Phi\right) \tag{3.15}$$

$$Z = ma_z = m\left(\dot{W} + PV - QU - g\cos\Theta\cos\Phi\right) \tag{3.16}$$

$$L = \dot{P}I_{xx} - \dot{R}I_{xz} + QR\left(I_{zz} - I_{yy}\right) - PQI_{xz} \tag{3.17}$$

$$M = \dot{Q}I_{yy} + PR\left(I_{xx} - I_{zz}\right) - R^2I_{xz} + P^2I_{xz} \tag{3.18}$$

$$N = \dot{R}I_{zz} - \dot{P}I_{xz} + PQ\left(I_{yy} - I_{xx}\right) + QRI_{xz} \tag{3.19}$$

These equations are highly non-linear because of the products of dependant variables, therefore it is convenient to categorize the whole motion of the aircraft into two parts, movement around one operating point (also called the trim value) and adding small increments of dynamic motion. To get the trim condition equations, it is important to note that the rates of change in trim conditions are implied and as such are equal to zero. The equations of motion for the trim conditions will be:

$$X_{trim} = m\left(Q_{trim}W_{trim} - R_{trim}V_{trim} + g\sin\Theta_{trim}\right) \tag{3.20}$$

$$Y_{trim} = m\left(R_{trim}U_{trim} - P_{trim}W_{trim} - g\cos\Theta_{trim}\sin\Phi_{trim}\right) \tag{3.21}$$

$$Z_{trim} = m\left(P_{trim}V_{trim} - Q_{trim}U_{trim} - g\cos\Theta_{trim}\cos\Phi_{trim}\right) \tag{3.22}$$

$$L_{trim} = Q_{trim}R_{trim}\left(I_{zz} - I_{yy}\right) - P_{trim}Q_{trim}I_{xz} \tag{3.23}$$

$$M_{trim} = P_{trim}R_{trim}\left(I_{xx} - I_{zz}\right) - R_{trim}^2 I_{xz} + P_{trim}^2 I_{xz} \tag{3.24}$$

$$N_{trim} = P_{trim}Q_{trim}\left(I_{yy} - I_{xx}\right) + Q_{trim}R_{trim}I_{xz} \tag{3.25}$$

The small dynamical increments are obtained by differentiating equations 3.14 to 3.19 and introducing the symbolism $dU = u$ for the right hand side parameters:

$$dX = m\left[\dot{u} + W_{trim}q + Q_{trim}w - V_{trim}r - R_{trim}v + \left(g\cos\Theta_{trim}\right)\theta\right] \tag{3.26}$$

$$\begin{aligned} dY = m\,[&\dot{v} + U_{\mathrm{trim}}r + R_{\mathrm{trim}}u - W_{\mathrm{trim}}p - P_{\mathrm{trim}}w - \\ &- \phi\left(g\cos\Theta_{\mathrm{trim}}\cos\Phi_{\mathrm{trim}}\right) + \theta\left(g\sin\Theta_{\mathrm{trim}}\sin\Phi_{\mathrm{trim}}\right)] \end{aligned} \tag{3.27}$$

$$\begin{aligned} dZ = m\,[&\dot{w} + V_{\mathrm{trim}}p + P_{\mathrm{trim}}v - U_{\mathrm{trim}}q - Q_{\mathrm{trim}}u + \\ &+ \phi\left(g\cos\Theta_{\mathrm{trim}}\sin\Phi_{\mathrm{trim}}\right) + \theta\left(g\sin\Theta_{\mathrm{trim}}\cos\Phi_{\mathrm{trim}}\right)] \end{aligned} \tag{3.28}$$

$$dL = \dot{p}I_{xx} - \dot{r}I_{xz} + \left(Q_{trim}r + R_{trim}q\right)\left(I_{zz} - I_{yy}\right) - \left(P_{trim}q + Q_{trim}p\right)I_{xz} \tag{3.29}$$

$$dM = \dot{q}I_y + \left(P_{trim}r + R_{trim}p\right)\left(I_{xx} - I_{zz}\right) - \left(2R_{trim}r - 2P_{trim}p\right)I_{xz} \tag{3.30}$$

$$dN = \dot{r}I_{zz} - \dot{p}I_{xz} + \left(P_{trim}q + Q_{trim}p\right)\left(I_{yy} - I_{xx}\right) + \left(Q_{trim}r + R_{trim}q\right)I_{xz} \tag{3.31}$$

As already said, this approach implies that the full motion is described by adding small dynamic increments to the trim conditions of the aircraft, therefore the full motion is described by $X = X_{trim} + dX$, $Y = Y_{trim} + dY$, $Z = Z_{trim} + dZ$ for longitudinal motion and $L = L_{trim} + dL$, $M = M_{trim} + dM$ and $N = N_{trim} + dN$ for lateral motion.

From this point, only the lateral motion will be considered since the goal of this thesis is to analyze the rolling motion specifically. Thus, the complete rolling motion of the aircraft is described by addition of equations 3.17 and 3.29:

$$\begin{aligned} L = \dot{p}I_{xx} - \dot{r}I_{xz} + &\\ + \left(I_{zz} - I_{yy}\right)&\left(Q_{\mathrm{trim}}R_{\mathrm{trim}} + Q_{\mathrm{trim}}r + R_{\mathrm{trim}}q\right) - \\ - I_{xz}&\left(P_{\mathrm{trim}}Q_{\mathrm{trim}} + Q_{\mathrm{trim}}p + P_{\mathrm{trim}}q\right) \end{aligned} \tag{3.32}$$

The impact aerodynamic forces are making is not included in the equation 3.32.

3.1.2 Aerodynamic forces and moments

If the aircraft is moving in any way through the fluid, it will create a reactive force of the fluid on the aircraft. In steady horizontal flight those reactive forces arise because of the relative motion of the aircraft to the air and/or the flow of accelerated air as a result of the propulsion system. A different approach can be defined for aircraft moving through air at very low speeds, i.e. helicopters or VTOLs. The resulting aerodynamic forces can be considered to be equal to force and moment changes which are the consequences of perturbations

from the trim condition. Those perturbations can be considered to be in nature similar to aerodynamic forces during steady flight.

Firstly, the equations that define aerodynamic forces and moments acting on the airplane in flight are:

$$X_a = \frac{1}{2} C_x \rho V_a^2 S \tag{3.33}$$

$$Y_a = \frac{1}{2} C_y \rho V_a^2 S \tag{3.34}$$

$$Z_a = \frac{1}{2} C_z \rho V_a^2 S \tag{3.35}$$

$$L_a = \frac{1}{2} C_l \rho V_a^2 S b \tag{3.36}$$

$$M_a = \frac{1}{2} C_m \rho V_a^2 S b \tag{3.37}$$

$$N_a = \frac{1}{2} C_n \rho V_a^2 S b \tag{3.38}$$

Equations 3.33 to 3.35 represent aerodynamic forces along their respective axes and equations 3.36 to 3.38 represent moments as a consequence of those forces. The coefficients C_i are dimensionless coefficients similarly to the *lift and drag coefficients* but different in value. If the lift and drag force are transformed into the body fixed coordinate system, the result will be the forces described by equations 3.33 to 3.35 and the coefficients would relate to each other accordingly. The velocity V_a is the speed of the aircraft relative to the fluid/air.

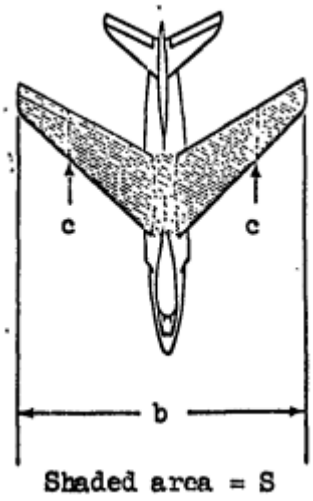

Figure 3.2: Graphical representation of the geometrical parameters[17]

The parameters S, b and c are shown graphically on figure 3.2. They are the wing area, wing span and mean aerodynamic chord respectively.

From these equations it can be concluded that the aerodynamic forces and moments are dependent on air density and the relative velocity to the fluid V_a. On the other hand, the dimensionless coefficients are functions of the Reynolds number, Mach number, angle of attack, angle of sideslip, the linear and angular velocities and their derivatives. Introducing the assumption that the aerodynamic forces and moments are linear functions of all mentioned variables around a certain point, in this case the trim condition, then the aerodynamic forces and moments can be expressed in a general sense in the form of a Taylor expansion:

$$F = F_{trim} + \left(\frac{\partial F}{\partial \Lambda_1}\right)_{trim} \lambda_1 + \left(\frac{\partial F}{\partial \Lambda_2}\right)_{trim} \lambda_2 + \left(\frac{\partial F}{\partial \Lambda_3}\right)_{trim} \lambda_3 + \dots \quad (3.39)$$

where Λ_i are the variables, including their derivatives, and λ_i are the perturbations (small increments of the variables). Higher order derivatives are neglected because the perturbations are considered to be small enough.

The introduced small perturbations λ_i are, however, relative to the atmosphere and not to the inertial space. Taking into consideration the nonuniform effects of the atmosphere, like wind gusts, those small atmospheric perturbations then equal to:

$$\lambda_a = \lambda - \lambda_g \quad (3.40)$$

where λ_g is the change in the variables of interest as a result of wind gusts and similar. Furthermore, the variables of interest for rolling motion are the lateral linear velocity and its derivative, the roll rate and the yaw rate. Combining equations 3.39 and 3.40 and picking only the mentioned variables of interest, the perturbation in the rolling moment can be written as:

$$dL = \frac{\partial L}{\partial V}(v - v_g) + \frac{\partial L}{\partial \dot{V}}(\dot{v} - \dot{v_g}) + \frac{\partial L}{\partial P}(p - p_g) + \frac{\partial L}{\partial r}(r - r_g) + \sum \frac{\partial L}{\partial \delta}\delta \quad (3.41)$$

where the last term, the sum, consists of control inputs like elevator deflection, aileron deflection, throttle increase, or, as it will be in this case, the momentum exchange with the reaction wheel, i.e. the influence of the reaction wheel on the torque exhibited on the aircraft. The equation 3.41 represents the full aerodynamic impact on the rolling motion, taking into consideration introduced assumptions.

3.1.3 Complete rolling motion equation of the aircraft

The equation 3.32 did not take into consideration the aerodynamic forces and that will be corrected. Here, another assumption is introduced and that is *zero trim conditions*. That means all the parameters with the subscript *trim* will be equal to zero. This is a usual approach to studying the impact of small changes in variables during either horizontal flight or in hover mode. Also, it is important to define the *dimensional stability derivative* in the form of:

$$\frac{1}{I_{ij}} \frac{\partial L}{\partial \Lambda} \lambda \quad (3.42)$$

and substitute it with the notation $L_\lambda\lambda$. the dimensional stability derivative is assumed to represent *all* the relative interactions of the atmosphere and the aircraft. By equating the equations 3.29 and 3.41 the *full* rolling motion of the aircraft is described by:

$$\dot{p} - \frac{I_{xz}}{I_{xx}}\dot{r} = L_v(v - v_g) + L_{\dot{v}}(\dot{v} - \dot{v_g}) + L_p(p - p_g) + L_r r + \sum L_\delta \delta \quad (3.43)$$

3.2 Reaction wheel subsystem coupled with the aircraft subsystem

As described in previous chapters, the reaction wheel subsystem while rotating will initiate momentum exchange with the aircraft subsystem. The reaction wheel is rotating on a shaft connected to a brushless DC motor, therefore it is convenient to describe the rotating motion of the wheel with the dynamical equation of a DC motor:

$$J_{rw}\dot{p}_{rw} = \frac{N}{R}(V - Np) + \tau_F \quad (3.44)$$

where J_{rw} is the moment of inertia of the reaction wheel, p is the roll rate, i.e. the rotational speed of the reaction wheel, N is the back-EMF of the motor, V is the voltage of the motor armature, R is the armature resistance and τ_F is the bearing friction force.

The control input to the reaction wheel is torque and the armature current of the BLDC motor is related to the input torque through the motor torque constant, which is equal to the inverse of the back-EMF.

The equation 3.44 can be rewritten as a function of the armature current:

$$\dot{p}_{rw} = -\frac{N}{J_{rw}}i - \frac{1}{J_{rw}}\tau_F \quad (3.45)$$

where the armature current is defined by equation[18]:

$$Ri = e - N(p - p_{rw}) \quad (3.46)$$

This equation couples the rolling rate of the reaction wheel and the aircraft.

To write the equation for rolling motion of the coupled system further assumptions are needed. The assumptions regarding the aircraft dynamics are possible because hover mode is assumed:

1. The only control input to the aircraft rolling motion equation 3.43 is the momentum exchange between the aircraft and the reaction wheel, i.e. the torque produced by the reaction wheel rotation
2. All the terms that describe the atmospheric influence in equation 3.43 will be equal to a certain disturbance torque
3. The moment of inertia cross products, i.e. the elements which are not on the main diagonal, are considered to be zero

4. It is assumed that the aircraft does not yaw, meaning, the yaw rate is assumed to be zero

5. The reaction wheel bearing friction is neglected, i.e. $\tau_F = 0$

Thus, by multiplying the equation 3.43 and having in mind that:

$$\sum L_\delta \delta = -J_{rw}\dot{p}_{rw} = Ni \tag{3.47}$$

and:

$$L_v(v - v_g) + L_{\dot{v}}(\dot{v} - \dot{v_g}) + L_p(p - p_g) = \tau_D \tag{3.48}$$

the rolling motion equation for the coupled system of the aircraft and reaction wheel becomes:

$$I_{xx}\dot{p} = -J_{rw}\dot{p}_{rw} + \tau_D \tag{3.49}$$

The equation 3.49 will be used for the analysis of the behavior of the coupled system in simulation.

Chapter 4

Simulation

4.1 Reaction wheel stabilization

Simulation was done using equations in the previous chapter and MATLAB Simulink. Dynamics of the eVTOL aircraft and the reaction wheel and DC motor subsystem have been made as separate dynamics blocks, but are coupled through their angular accelerations, as seen in equation 3.49.

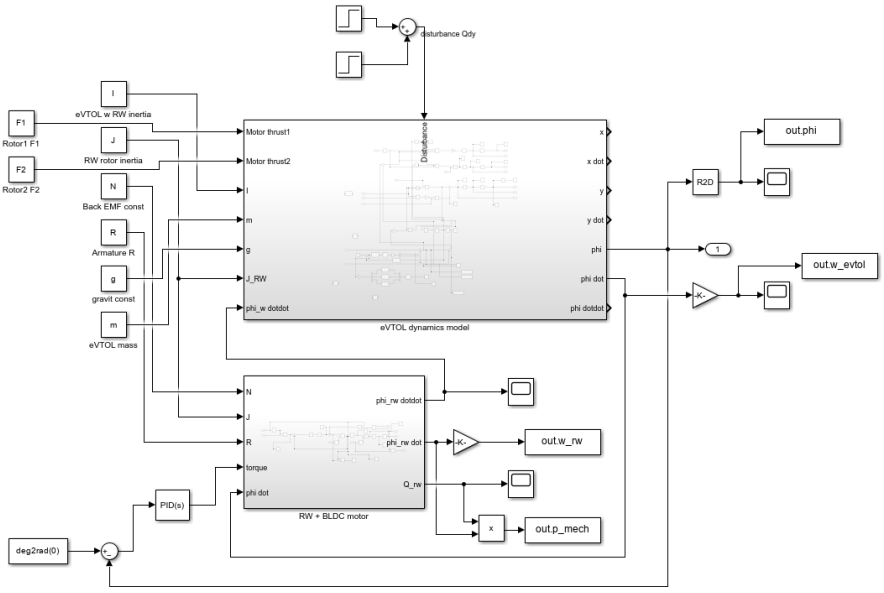

Figure 4.1: Block structure of the whole system in Simulink

The block structure of the whole system is shown in figure 4.1. It consists of two subsystems: the dynamics of the eVTOL aircraft and the reaction wheel and DC motor subsystem. The input parameters have been talked about in previous sections. Beside them, the angular acceleration of the aircraft subsystem is coupled with the reaction wheel subsystem through their respective angular accelerations. For the purposes of this simulation, the output of interest is the roll angle. A more detailed block structure of the aircraft subsystem is shown in figure 4.2.

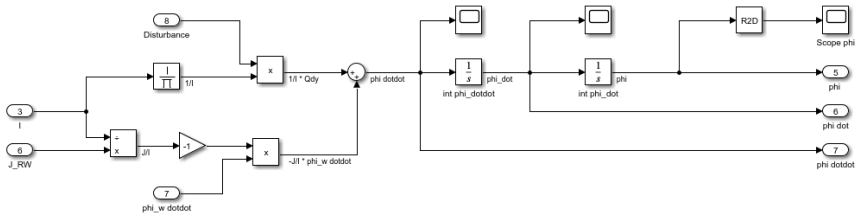

Figure 4.2: Block structure of the aircraft subsystem in Simulink (rolling motion)

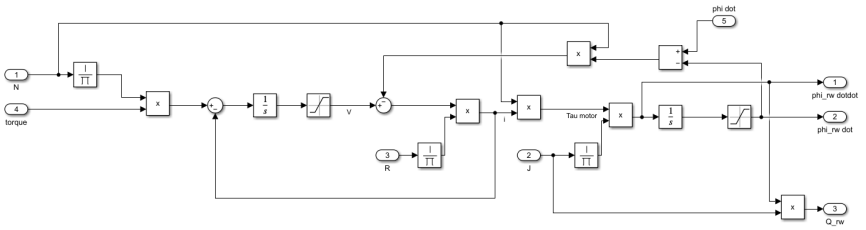

Figure 4.3: Block structure of the reaction wheel subsystem in Simulink

The block structure of the other subsystem, reaction wheel and DC motor subsystem, is shown in figure 4.3. For simulation purposes, certain motor parameters are needed:

- The back-EMF $N = 0.2167 Vs/rad$
- Armature resistance $R = 1\Omega$
- Torque-current constant (equal to back-EMF) $k_T = 0.2167 Nm/A$

These specific values were used because some real life examples of high power DC motors used in the aerospace industry are similar to them[19]. The physical parameters of the reaction wheel depend, as previously analyzed, on the material used. Here, only the medium and high performance grade will be taken into consideration. Their respective moments of inertia have been listed in the previous section.

The reaction wheel subsystem is used for roll control. The control input is the torque that should be generated on the shaft the reaction wheel is rotating with. It is obtained as the output of a PD regulator. The input of the regulator is the roll angle difference between the current roll angle of the aircraft and the reference value which is zero in this casse. The parameters of the PD regulator are obtained through *rltool* in MATLAB. The root locus graph is shown on figure 4.4. The proportional gain of the controler is $K_P = -2.83$ and the derivative parameter $K_D = -590$.

The goal of the simulation is to observe the behavior of the whole system during the already talked about simple stabilizing test maneuvre. All the initial conditions are set to zero, except the initial roll angle of the aircraft, which is 10°. Since stabilization is the goal, the reaction wheel subsystem is

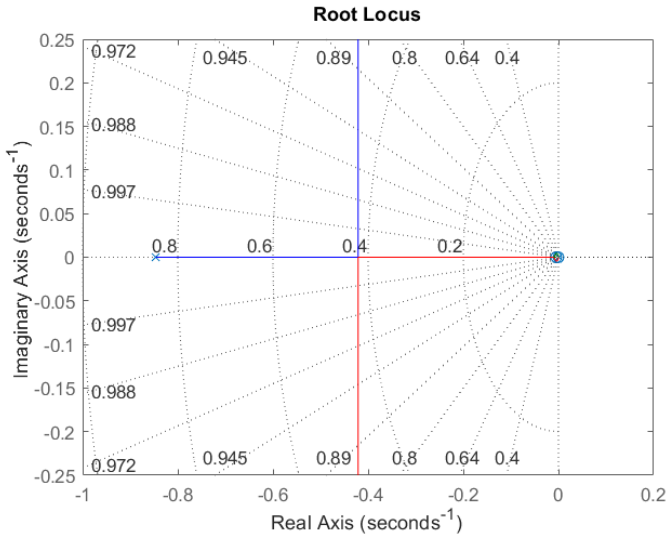

Figure 4.4: Root locus graph of the RW stabilization system

used to generate a change in angular momentum which stabilizes the whole aircraft to 0°.

The medium performance grade reaction wheel has a moment of inertia of $I_{rw} = 0.1692261kgm^2$ and a mass of $m = 4.1553kg$. Together with the motor, which has a mass of approximately $15kg$, the whole subsystem would weigh around $20kg$. The response of the controlled system is shown on figure 4.5.

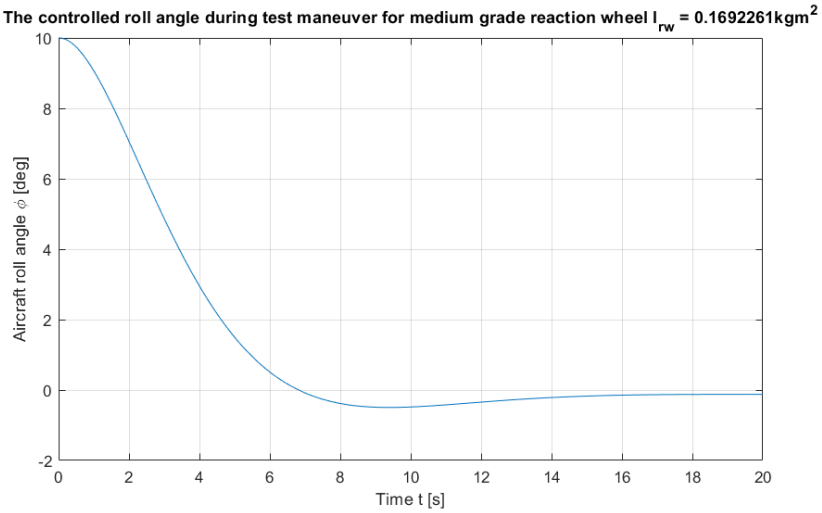

Figure 4.5: Roll angle of the aircraft as a function of time - medium grade

The reaction wheel subsystem manages to stabilize the aircraft inside of the wanted stabilization interval of 10 seconds. It reaches 10% of the initial roll angle (and stays inside the 10% range) in about 6 seconds from the start, which is the settling time of the system. Overshoot is almost nonexistent,

being 5%, which is around 0.5°.

The angular velocity of the reaction wheel and the aircraft during the stabilization maneuver is shown in figure 4.6

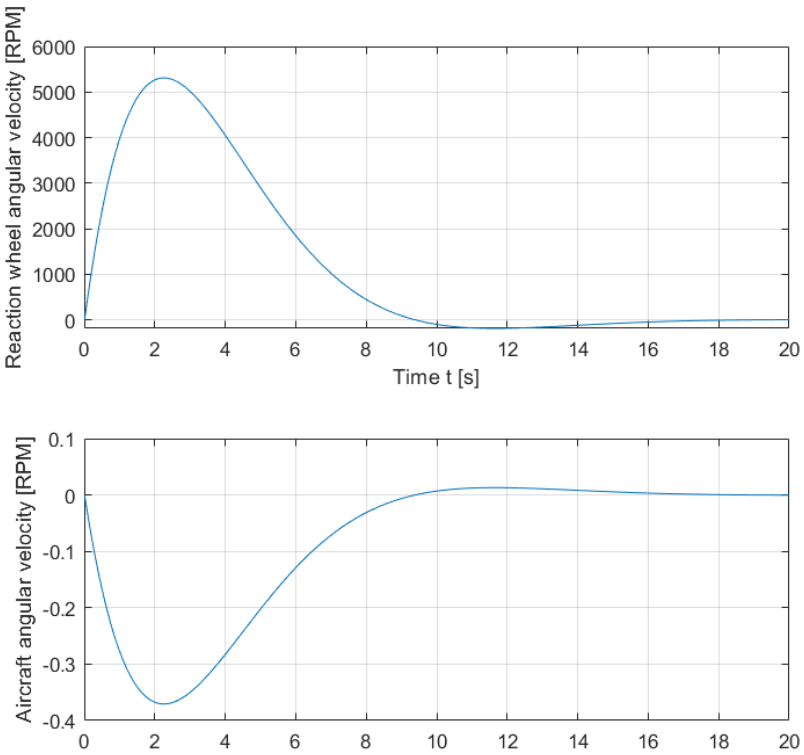

Figure 4.6: Angular velocities of the reaction wheel and aircraft - medium grade

Important to see in figure 4.6 is the exchange of angular momentum shown in equation 2.2 between the reaction wheel and the aircraft, visible in the opposite signs of their respective velocities. As a comparison with the previous analysis in chapter 2, comparing the peak value of the angular velocity of the medium grade reaction wheel with the value in 2.2, it can be seen that the expected output and simulation output are similar, withing a margin of around 5%.

The mechanical power of the shaft is shown in figure 4.7. Again, by comparing the mechanical power excerted by the shaft with the expected value in 2.2 for the medium grade reaction wheel, it can be seen that they lie within a margin of 15%, which provides usefull insight into the previous analysis. Still, a much bigger margin should be included into the choice of the BLDC motor, as previously said.

The reaction wheel of higher grade has a moment of inertia of $I_{rw} = 0.3062916kgm^2$ and a mass of $m_{rw} = 7.52097kg$, so together with the motor, the mass is around $m = 22.5kg$. The controlled roll angle output for a high grade reaction wheel is shown in figure 4.8. The same PD controller was used in this case as in the previous one. The response of the system is about the

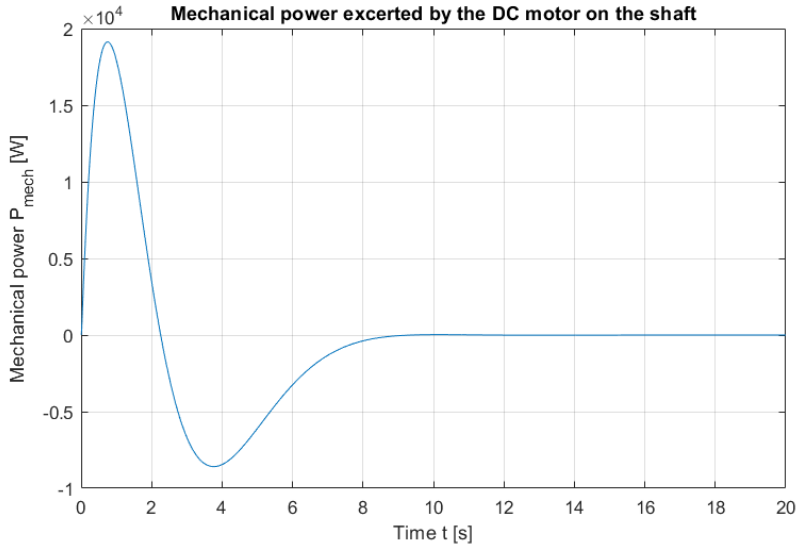

Figure 4.7: Medium grade reaction wheel - mechanical power on the shaft

same, only the overshoot is even lesser in this case, being less than 1%. The expected and simulated peak values of the higher grade reaction wheel (see table 2.2) angular velocities lie within a margin of 5%, which gives further positive insight into the analysis from chapter 2. The angular velocities for the higher grade reaction wheel and aircraft can be seen in figure 4.9. Even the peak required mechanical power corresponds to the expected value within a margin of less than 5%, as can be seen in figure 4.10

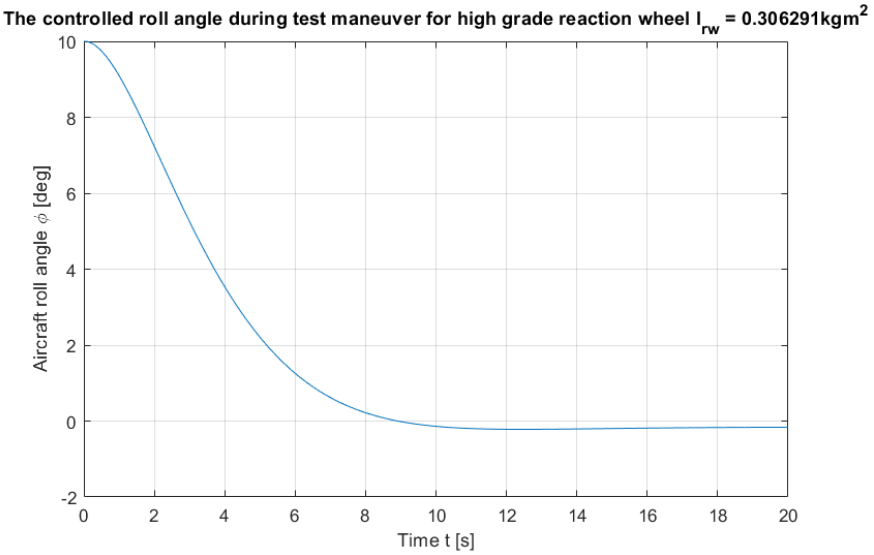

Figure 4.8: Roll angle of the aicraft as a function of time - high grade reaction wheel control

Both the medium grade and higher grade reaction wheels managed to

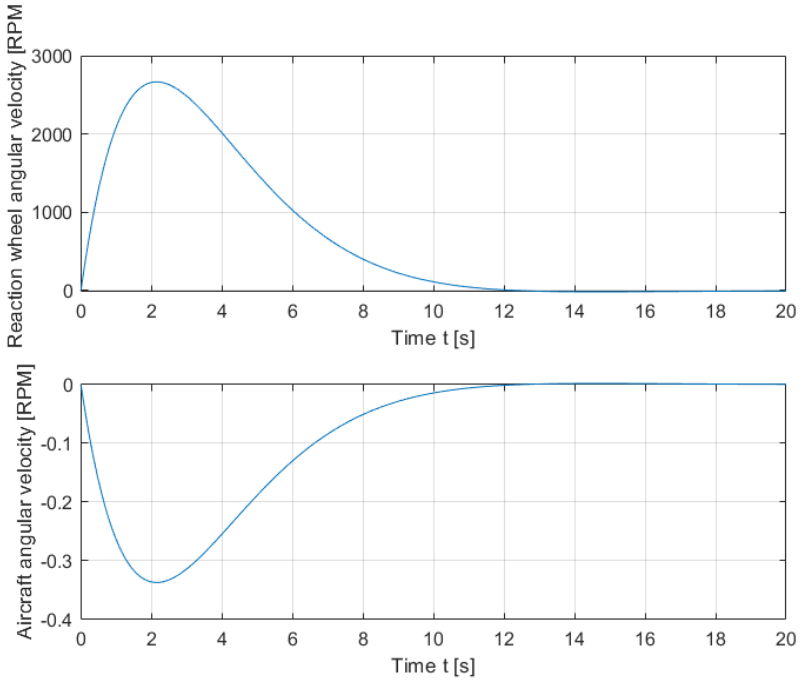

Figure 4.9: Angular velocities of the reaction wheel and aircraft - high grade reaction wheel

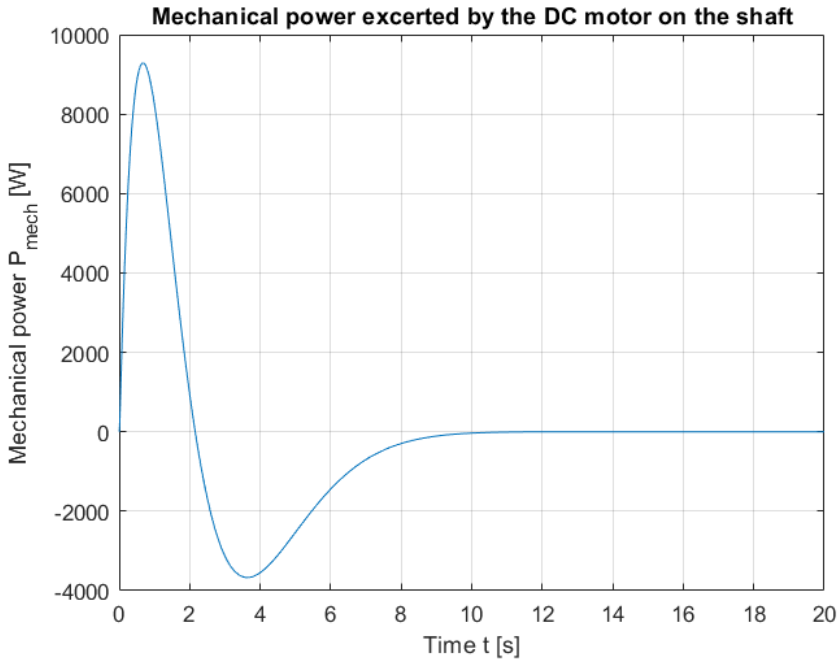

Figure 4.10: High grade reaction wheel - mechanical power on the shaft

stabilize the aircraft inside the given time interval, but what is important, is that the required power for such a maneuver is halved by using higher performance grade materials in the construction of the reaction wheel. The negative side of that is the weight. Choosing higher performance grade materials over medium grade ones brings with it an additional 12.5% increase in mass, which is an additional $2.5kg$ for a reaction wheel of the previously defined volume and geometry.

4.1.1 Optimization of reaction wheel parameters

In this section, it has been shown how a reaction wheel of different material grades but for a specific predefined geometry can be used for the roll angle stabilization of an eVTOL aircraft in hover mode. If we focuse only on one material grade, for example, the higher grade material, the results imply an increase in mass by about $22.5kg$ which is substantial considering the overall size of the aircraft. This, however, can be optimized, since according to the chapter 2 *Materials* analysis, the maximum angular velocity of the higher grade reaction wheel is $\omega_{max} = 49312RPM$, therefore, that reaction wheel is able to generate a maximum angular momentum of $L_{max} = 1581.6831Nms$ which is far beyong what is needed for the test manoeuvre ($L_{required} = 84.6205$, see chapter 2). Since the disparity between the required and maximum possible angular momentum is that big, it is natural to consider both a reduction in reaction wheel mass (ergo, the moment of inertia) and the power level of the BLDC motor, which would also decrease the motor mass.

Similar to the derivation of the equation 2.24, and according to [12], for a specified test manoeuvre defined by the total roll angle displacement $\Delta\theta$ of the aircraft with moment of inertia I lasting for a total of Δt seconds, with constraints put on the reaction wheel design: the maximum angular velocity of the reaction wheel ω_{max} and the maximum available power of the BLDC motor P_{max}, an equation for the necessary reaction wheel moment of inertia can be derived:

$$I_{rw} = \frac{\Delta t P_{max} - \sqrt{\Delta t_{max}^2 P^2 - w\omega_{max}\Delta\theta IP}}{\omega_{max}^2} \tag{4.1}$$

The constraints put on the reaction wheel desing are predefined and depend on the use case scenario. In the section above, in the simulation a BLDC motor able to produce output power of $100kW$ was used, therefore, for this part it is assumed, that the maximum available power for the task is $50kW$, which would more than halve the weight of the motor to approximately $10kg$. When it comes to the angular velocity of the reaction wheel, simulation data showed, the already analyzed reaction wheel developed a maximum angular velocity of approximately 2700 RPM. The goal now is to increase the maximum angular velocity for the same test manoeuvre which will, according to 4.1, reduce the reaction wheel moment of inertia, thus reducing the mass of the reaction wheel. The expected maximum angular velocity of the reaction wheel will be assumed to be $\omega_{max} = 5000RPM$.

Now, having all the necessary parameters and constraints defined, for the same test manoeuvre as before, the necessary reaction wheel moment of inertia is:

$$I_{rw} = 0.0827 kgm^2 \tag{4.2}$$

which is, when comparing to 2.14, a substantial reduction. If we assume the same geometry as before, meaning, the reaction wheel is a ring with the outter radius of $150cm$ and inner radius 90% of that, $13.5cm$, with all of its mass concentrated in the outter part, then the mass would be:

$$m_{rw} = \frac{2I_{rw}}{R_1^2 + R_2^2} = 1.05kg \tag{4.3}$$

Recall, in the section above, the mass of the ring was around $7kg$. Therefore, it is safe to assume, that an improvement has been made, since the total weight of the system now is around $11kg$ as opposed to before, which was around $20kg$.

To show the comparative behaviour of the system in the simulation, the same PD controller was used and the rotation of the motor shaft was limited to $5000RPM$. In figure 4.11, the stabilization manoeuvre is shown, now

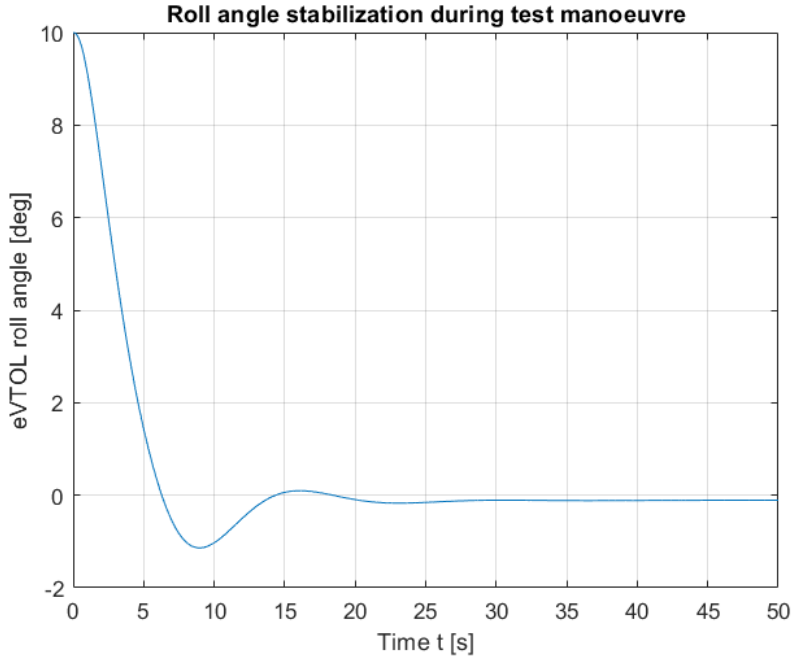

Figure 4.11: Optimized reaction wheel: eVTOL roll angle as a function of time

using the improved reaction wheel parameters. The settling time is still acceptable since the settling time is around the expected 10 seconds interval. The only difference is the slightly bigger overshoot of around 9% which could be improved but for the price of a slower response. Also, important to note is, that it is possible to further improve the response time to less than 10 seconds, which would increase the overshoot. For this purpose, overshoot

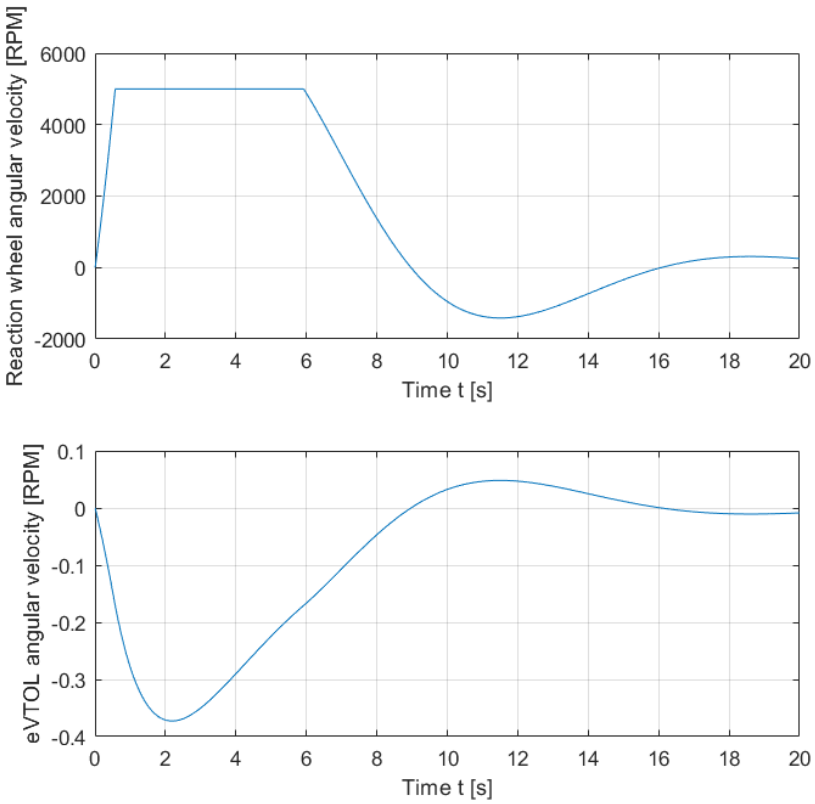

Figure 4.12: Optimized reaction wheel: angular velocities

is wanted to be held at minimum. The velocities of this renewed reaction wheel design and eVTOL are shown in figure 4.12. It is noticeable, that the reaction wheel reaches its predefined maximum angular velocity. From a construction perspective, it is still inside the safety zone, since the maximal allowed angular velocity of the wheel itself is dependend on the choice of materials and geometry. This maximum value is less than the calculated value in the sections above, which is $\omega_{max} = 49000RPM$ for the higher grade material, so a significant safety margin already exists when it comes to the constructional stability. The high grade material has a rather high range of allowed angular velocities, most of which in reality will never be reached.

The reaction wheel angular velocity is mainly constrained by the motor used for its functioning, so it is natural to also look at the mechanical power output of the motor shown in figure 4.13. As defined above, the assumed available power source is rated at $50kW$ maximum. The moment the reaction wheel reaches its peak angular velocity, the simulation yields the peak power requirement of around $42kW$, which is close to the expected value. Here, safety margins should be considered with the choice of the motor, since the safety margin is only 16%.

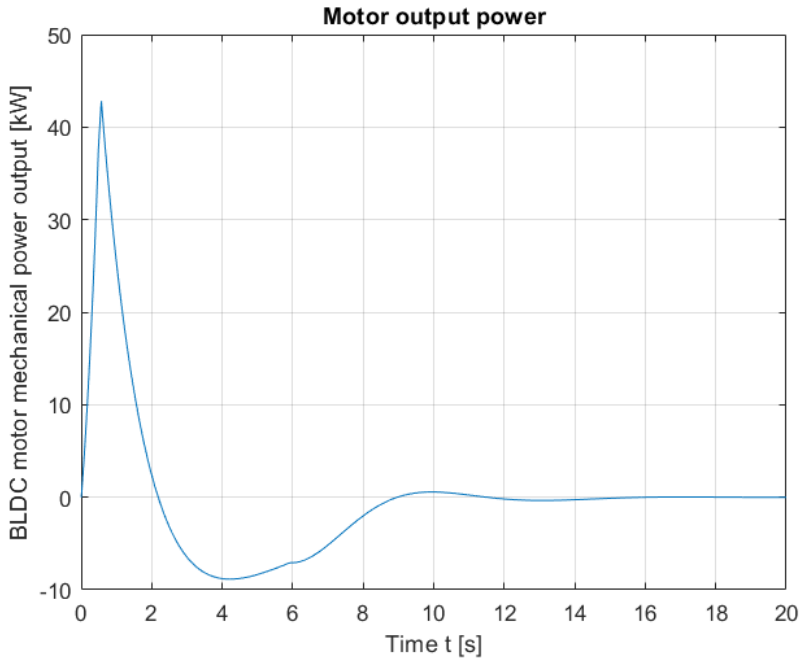

Figure 4.13: Optimized reaction wheel: motor mechanical power output

4.2 Differential thrust stabilization

A more conventional method of hover flight stabilization is the application of differential thrust to symmetrically placed propulsors on the lateral axis of the aircraft. To assure the aircraft stays in hover mode, the differential thrust is applied to the equilibrium state value of thrust made by the propulsors which should be equal to the weight of the eVTOL system. A free body diagram is shown on figure 4.14. It is assumed, that the propulsors are placed symmetrically on the ends of each wing, where the wingspan is $2L$. This changes the equation for the rolling motion 3.49 in the following way:

$$I_{xx}\dot{p} = (T_1 - T_2)\, L + \tau_d \tag{4.4}$$

The amount of differential thrust that is needed to be applied depends on the roll angle, $\Delta T = f(\theta)$ and it will go to zero as θ goes to zero, leaving the aircraft in the equlibrium hover state $T_1 + T_2 = mg$. The block structure of the differential thrust stabilization system is shown in figure 4.15. The propulsors on the ends of wings are thought to be propellers attached to their respective motors. The propellers' inertia is simulated with the block with the transfer function:

$$G(s) = \frac{1}{\tau s + 1} \tag{4.5}$$

where τ is the time constant. For this analysis the time constant is assumed to be equal to 1 second.

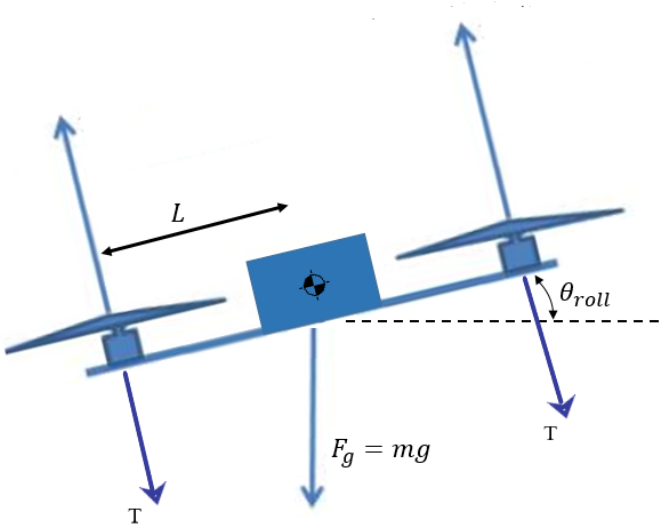

Figure 4.14: Free body diagram during rolling motion

For both propulsors the same PD controller is used, where $K_P = 0.5$ and $K_D = 49$. The values were chosen with help of the *rltool* functionality in MATLAB. The root locus graph is shown in figure 4.16.

As a means to comparing this conventional stabilization method to the one in section 3, the same test manoeuvre is used, i.e. a stabilization manoeuvre from an initial roll angle of 10° to 0° in 10 seconds.

Like it was previously introduced, this method relies on creating differential thrust by the rotors to stabilize the roll angle of the aircraft. Incorporating the controller as it is shown in figure 4.15, the thrust produced by the rotors during the manoeuvre as a function of time can be seen in figure 4.17. The points of interest lie in the peak values on the graph. Thrust increase on one of the propulsors is only 0.1% of the equilibrium, which indicates a much more economic solution compared to the stabilization method that includes a reaction wheel. If the propulsors were fuel based, meaning, if the motors, because of which the propellers rotate, were not electric, even a 0.1% increase would be significant. The thrust produced by one propulsor during hover mode is equal to $3688N$, a 0.1% increase results in a thrust of $3691N$ which is an increase of approximately $3N$. If we look at the specific fuel consumption of a turbojet engine, for example the *J-79-GE-119*[20], it is equal to $0.198kgN^{-1}h^{-1}$, every 10 seconds an additional 1.7 grams of fuel will be lost. This becomes non-negligible after many such manoeuvres, but still of no great importance.

Another comparison parameter is the settling time for this method and the reaction wheel stabilization. The reposnses of both stabilization methods is shown in figure 4.18. Both responses were gotten by using the already introduced control laws and constraints. The differential thrust method

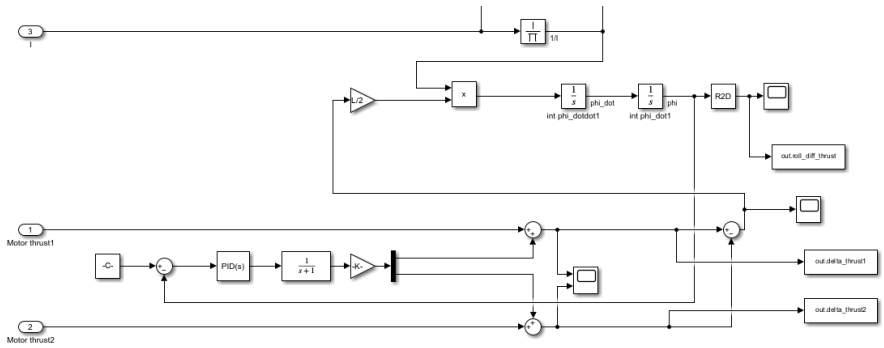

Figure 4.15: Thrust stabilization block structure

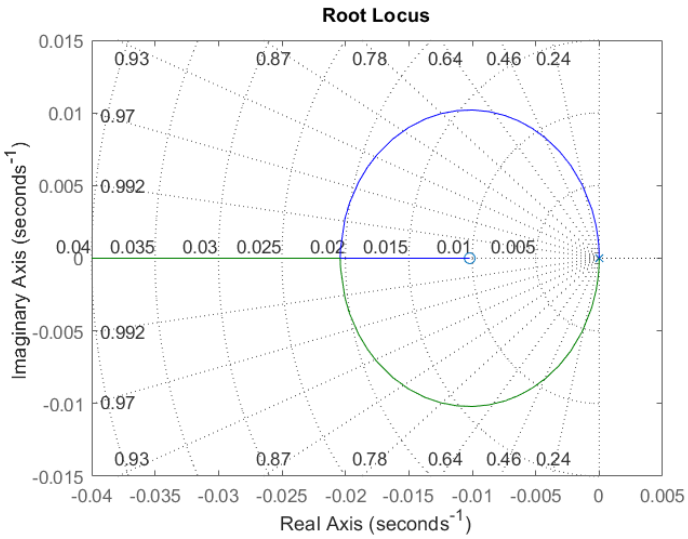

Figure 4.16: Root locus of the differential thrust system with PD controller

yielded a settling time of around 12 seconds, while the stabilization with a reaction wheel got to 10% of the initial value in about 6 seconds which shows a significant increase in stabilization speed. Other than that, there is a slightly bigger overshoot in the case of differential thrust stabilization.

4.3 Simulation with disturbances

In the previous section, the control laws for both stabilization techniques were based on PD regulation. Only proportional or proportional with integral component control laws produced an unstable system, but that is not the only reason why PD control was used. According to [21], the derivative component does not have many uses in fast response systems, because a, for example, 10% increase in response time for a fast response system is not detrimental. In this case, a eVTOL aircraft is quite inert in the sense of

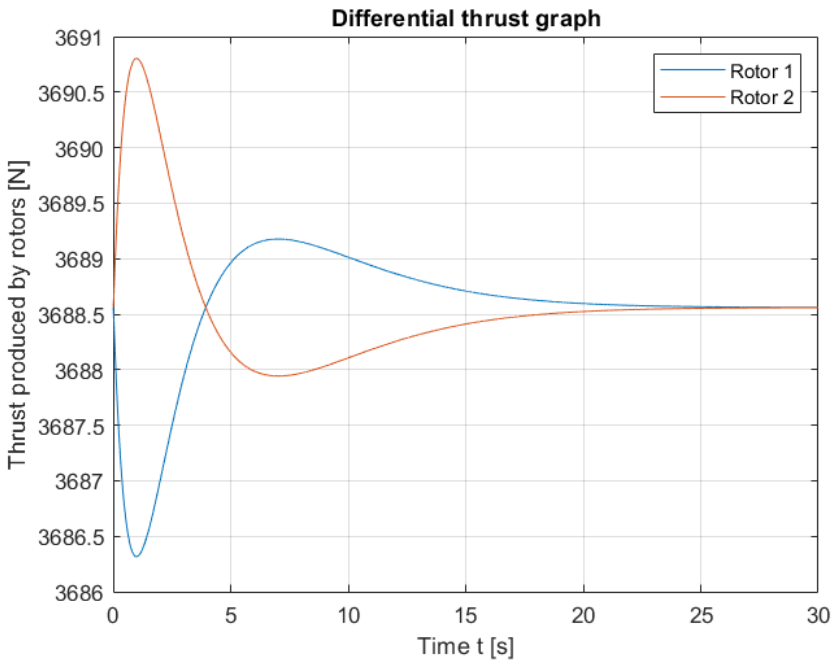

Figure 4.17: Thrust produced by the rotors

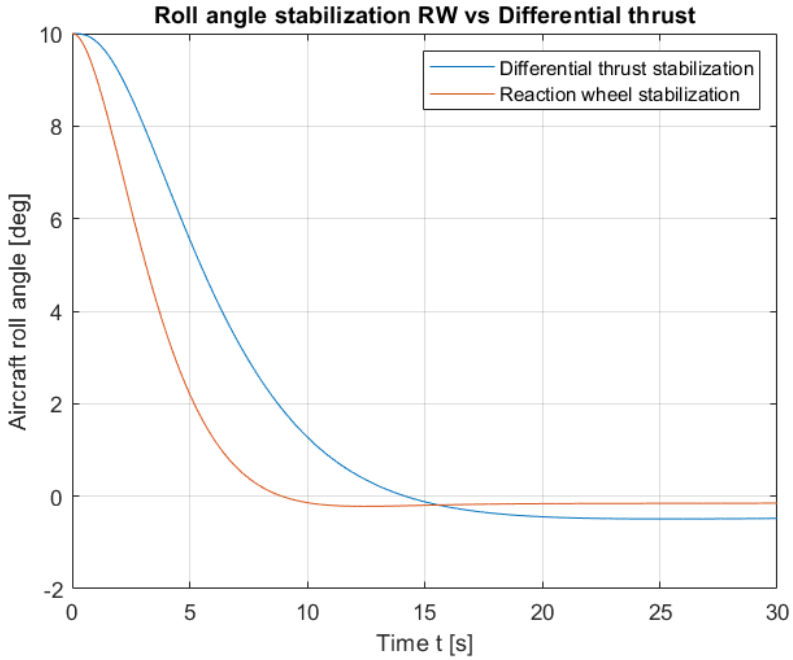

Figure 4.18: Roll angle stabilization

rolling motion so it falls into the category of not-so-fast-response systems. So since the requirements in the previous sections were mostly in the scope of a fast response and minimal overshoot, the derivative component was very big. The proportional-derivative control proved itself usefull for that analyzed use case where no disturbances were present. By assigning a non-zero value to the τ_D term in equation 3.49, the already used controllers did not produce a satisfying output, meaning, for different values of the disturbance torque, the steady state error was either too high or the system became unstable. The reason why is directly corelated to the big derivative component used in the controllers. When there is a disturbance, normally it is wanted for the system to recover quickly, but the derivative component dampens that. Therefore, in the presence of disturbances the need to increase both the proportional and integral components arises.

First the behavior of the reaction wheel stabilization system with different values of the disturbance torque will be analyzed. The values of each of the PID components are -120.83, -10 and -890 respectively. The disturbance torques are modelled as a constant disturbance during the whole window of observation, i.e. from the beginning to the end of the simulation. The response

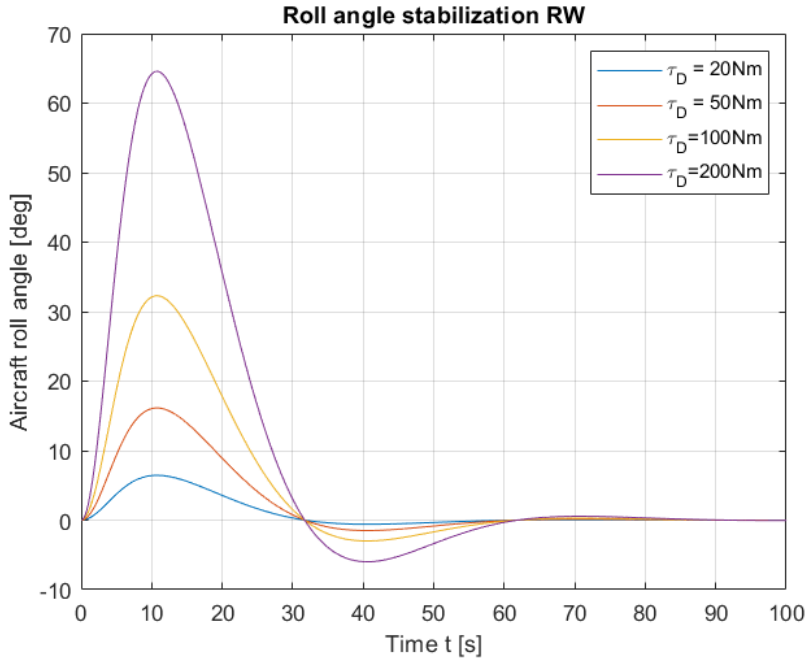

Figure 4.19: Roll angle stabilization with different values of disturbance torque (reaction wheel)

of the system using the reaction wheel mechanism for stabilization when under disturbance of a range of torque values is shown in figure 4.19. According to these results, it can be said that the maximum disturbance torque is expected to be around $200Nm$ because the initial displacement around the longitudinal axis becomes greater than $60°$ which is double the recommended maximum roll angle for passenger aircraft. Important to note is the behavior of the

reaction wheel itself. For the case of a constant disturbance, energy is being brought to the system continously which means the reaction wheel would keep increasing its angular rate in a linear manner. That obviously is not possible in real applications because, as it was already explained, the reaction wheel has a point at which it becomes saturated after which other mechanisms need to desaturate it and take on the stabilizing role. Even in spacecraft where the reaction wheels are commonly used, the outside disturbances are in amplitude nowhere near these tested values and rarely continous. The reaction wheel stabilization mechanism analyzed in this thesis could theoretically be used for stabilization manoeuvres, even in the presence of disturbance torques which are of finite duration and up to $200Nm$ in amplitude.

For comparison purposes, the behavior of the system in the case of differential thrust stabilization will be here analyzed also. Same as for the reaction wheel part, the PD control used in previous sections was not enough to stabilize the system with the presence of disturbances. The updated control law is a PID controller with components of 9.9, 0.5 and 73.4 respectively. In figure

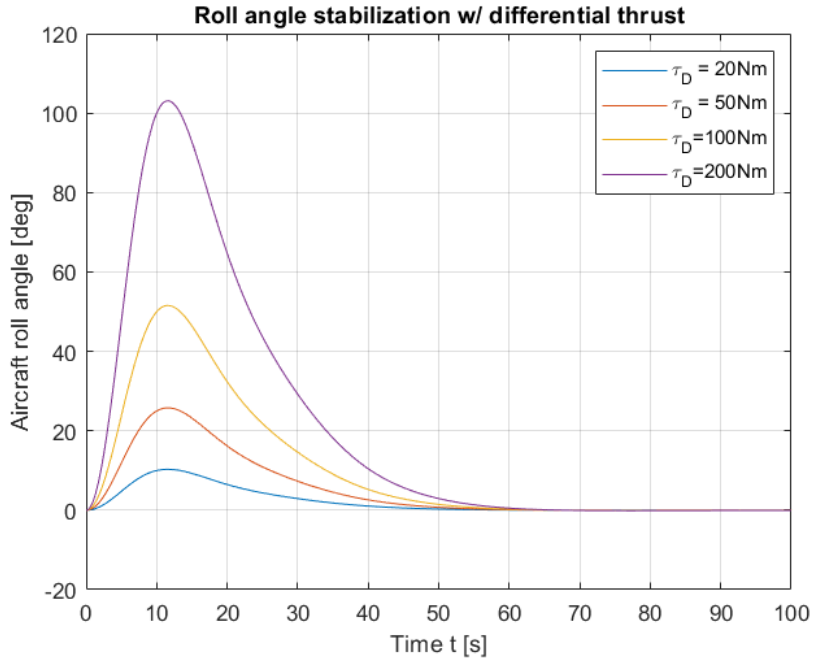

Figure 4.20: Roll angle stabilization with different values of disturbance torque (differential thrust)

4.20 the response of the system (block structure in figure 4.15) is shown, again for the same range of disturbance torques. Immediately noticeable is the initial roll angle displacement reaching 100° which is in reality not possible without catastrophic consequences. It is possible to tweak the controller (by increasing the proportional gain) so that the system does not "roll over" but that introduces oscilations in the response which is here not wanted. The time constant of the propulsion system in this case is $\tau = 1s$. It has a significant impact on the response of the system and as such will be tested for

different values. From figure 4.20 the maximum allowed disturbance torque will be taken as $\tau_D = 100Nm$. Therefore, the response for different time constants will be analyzed only in the case of disturbance torque equal to $20Nm$. The response for the time constants of $0.1s$, $1s$ and $1.5s$ is shown

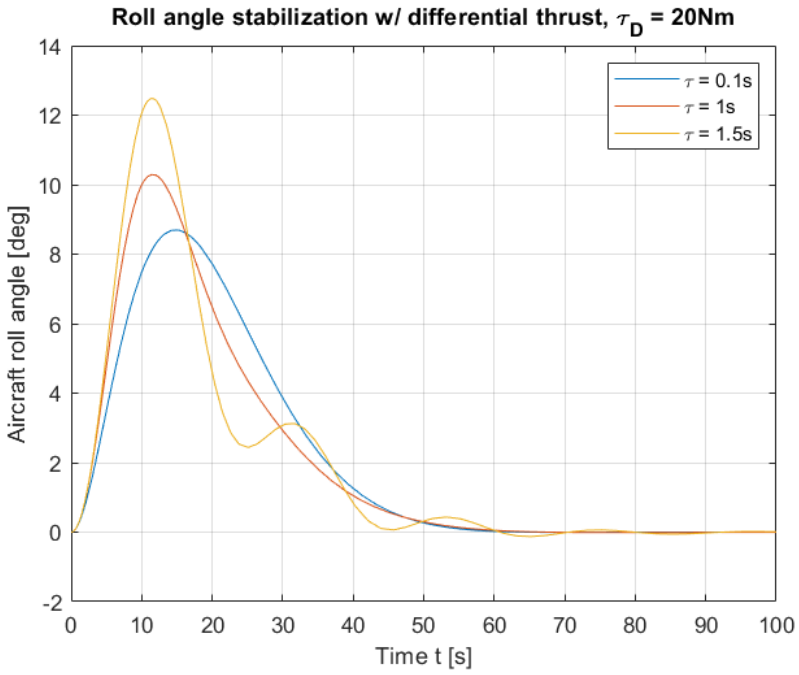

Figure 4.21: Roll angle stabilization with differential thrust for disturbance torque of 20Nm for different values of the time constant τ

in figure 4.21. The bigger the time constant is, the system is more sluggish in nature, therefore reacts slower to rapid changes as is the case with the disturbance here. Slower reaction is visible by the greater initial displacement. For the time constant of $\tau = 1.5s$ oscillations start to emerge which indicates that the system is becoming unstable and the introduced PID controller is not able to keep it stable. This shows the need for some other control method if the dynamics of the system may vary over time, like Model Predictive Control for example.

Comparing the developed control laws for both stabilization techniques, differential thrust and reaction wheel, where the stabilization times are approximately the same, it can be concluded that the reaction wheel stabilization reacts much better to sudden changes. That is important for this case since the sudden changes in reality could be wind gusts which are a product of a nonuniform atmosphere, therefore they vary in intensity. As shown, the reaction wheel mechanism is able to cover a greater range of disturbance torques preventing a catastrophic failure of the system.

Chapter 5

Results

From the simulations in the previous chapter many things can be concluded. First to be pointed out is the ability for the designed reaction wheel assembly to stabilize some theoretical description of a eVTOL aircraft inside of a simulation environment, which was in question beforehand. The simulations gave satisfying results for a simple test manoeuvre and also during constant disturbances of different intensities. However, the other point of interest is the energy comparison of such an assembly to the state-of-the-art stabilization techniques.

According to [3], the disck actuator theory defines the power required for the generation of thrust required to hover as a function of air density and propeller disk area as:

$$P = \sqrt{\frac{T^3}{2\rho A}} \tag{5.1}$$

If we assume that the analyzed eVTOL realization of the *Cessna 172* airplane has, as already assumed, two propulsors on the ends of wings with propeller disk area of $1.8m$, then the power required to hover, according to 5.1, would be $106.6758kW$. The simulated results, when it comes to power, showed the differential thrust stabilization increases from that value only slightly, even during constant disturbances with analyzed values.

On the other hand, the reaction wheel assembly during the test manoeuvre reached a peak of around $9kW$ of power needed from batteries. Those batteris would have some weight to them, and the BLDC and reaction wheel assembly would also add weight of around $16kg$. If we assume the batteries used have specific energy of $E_{spec} = 240Wh/kg$, then just for the assembly to be integrated to the eVTOL, another $3840Wh$ of energy capacity would need to be supplied via adding batteries.

Chapter 6

Conclusion

In chapter 1, certain goals of this thesis have been defined. After the simulations and tests, those goals are adressed in this chapter.

1. **Study the dynamics of eVTOL aircraft in hover mode and create an apropriate model**

   Through chapters 2 and 3 the dynamic aspect of eVTOL aircraft (and to some degree, aircraft in general) was thoroughly analyzed. The general mathematical model was afterwards tailored to fit the requirements of this thesis the best, i.e. hover mode, impact of wind gusts etc.

2. **Create a general reaction wheel model**

   In chapter 2, the full physical and mathematical description of a reaction wheel assembly was provided illustrating its core principles.

3. **Analyze the impact of different materials, which can be used for the reaction wheel design, on the stabilizing ability**

   Together with the physical description of the reaction wheel, materials analysis was done and different grades of materials have been compared between each other. The main criteria was the impact of a certain type of material on the stabilizing ability of the reaction wheel.

4. **Study the possibility of reaction wheel parameter optimization for a given use case**

   An approach to the optimization of reaction wheel physical properties was introduced. It was shown how a substantial reduction in mass and DC motor power requirement did not diminish the stabilizing ability of the assembly.

5. **Integrate the reaction wheel subsystem to the aircraft**

   In chapter 3 were the mathematical models of the eVTOL aircraft and the reaction wheel assembly coupled together, which defined new dynamics equations for the system as a whole.

6. **Compare the funcionality of the developed system with state-of-the-art stabilization techniques, like differential thrust stabilization**

The simulations showed certain aspects in which the reaction wheel assembly was superior over state-of-the-art stabilization techniques, presented in the 4th chapter. Improvements to the simulated results are possible through more advanced control law implementations.

7. **Analyze the power consumption for the whole system**

   After simulations the energy consumption and potential "mass costs", which are of great importance in aviation, were discussed in the 5th chapter as part of the simulation results.

In the end, it can be concluded that, analogously to spacecraft, even for stabilization of aircraft in hover mode reaction wheel assemblies might show usefullness. The ability of reaction wheels to be very precise means that they can react to very small disturbances detected by the measurement units on board of the aircraft, which has potential to greatly increase the comfort for passengers. There are possibilities for future work, especially with the advancements in power electronics giving improvements in the brushless DC motor sphere, making them even more compact and efficient. Likewise, the ever growing need for vehicles in general to switch to electric propulsion means constant improvement of battery technology. Advancements in those fields will open the door to further and more detailed investigation of reaction wheels as main stabilizers for hovering aircraft.

Bibliography

[1] Mike Hirschberg. *VTOL wheel of fortune*. https://evtol.news/news/commentary-electric-vtol-wheel-of-fortune. [Accessed 13-05-2024].

[2] *Technology | Zuri — zuri.com*. https://zuri.com/technology.

[3] Alessandro Bacchini. *Electric VTOL preliminary design and wind tunnel tests*. July 2020.

[4] *NASA Puffin Electric Tailsitter VTOL Concept - NASA Technical Reports Server (NTRS) — ntrs.nasa.gov*. https://ntrs.nasa.gov/citations/20110011311.

[5] Mark D. Moore. "Misconceptions of Electric Aircraft and their Emerging Aviation Markets". In: *52nd Aerospace Sciences Meeting*. DOI: 10.2514/6.2014-0535. eprint: https://arc.aiaa.org/doi/pdf/10.2514/6.2014-0535. URL: https://arc.aiaa.org/doi/abs/10.2514/6.2014-0535.

[6] *Mechanical Units, Low-Order Mechanical Systems, and Simple Transient Responses of First Order Systems*. Virginia Polytechnic Institute and State University, Mar. 2021.

[7] URL: https://aerospace.honeywell.com/us/en/about-us/blogs/understanding-reaction-wheels.

[8] Emre Sayin, Rahman Bitirgen, and Ismail Bayezit. "Attitude Control and Parameter Optimization: A Study on Hubble Space Telescope". In: *Measurement Science Review* 23.4 (2023), pp. 146–153. DOI: doi:10.2478/msr-2023-0019. URL: https://doi.org/10.2478/msr-2023-0019.

[9] M. Durgut. *Understanding Roll, Pitch, and Yaw: The Three Axes of Flight*. URL: https://www.aviationfile.com/roll-pitch-yaw-axes/.

[10] Marek Cel. "Cessna 172 Flight Simulation Data". In: (Dec. 2019). DOI: 10.13140/RG.2.2.27040.51205.

[11] Pushparaj Pathak, Amalendu Mukherjee, and Anirvan Dasgupta. "Attitude Control of a Free-Flying Space Robot using a Novel Torque Generation Device". In: *Simulation* 82 (Oct. 2006), pp. 661–677. DOI: 10.1177/0037549706074486.

[12] Abolfazl Shirazi and Mehran Mirshams. "Design and performance simulation of a satellite momentum exchange actuator". In: *Australian Journal of Mechanical Engineering* 14 (Jan. 2016), pp. 1–9. DOI: 10.1080/14484846.2015.1093223.

[13] E.A. Slejko. "Enhancing demisability without sacrificing performance: material selection for the case study of reaction wheels in the framework of design for demise". In: *Journal of Space Safety Engineering* 8.3 (2021), pp. 217–224. ISSN: 2468-8967. DOI: https://doi.org/10.1016/j.jsse.2021.06.001. URL: https://www.sciencedirect.com/science/article/pii/S2468896721000598.

[14] ASTROFEIN. URL: https://www.astrofein.com/en/reaction-wheels/rw6000/.

[15] Aerospace Specification Metals Inc. URL: https://asm.matweb.com/search/SpecificMaterial.asp?bassnum=mtp641.

[16] D.T. McRuer, I.L. Ashkenaz, and D. Graham. *Aircraft Dynamics and Automatic Control*. Princeton, New Jersey: Princeton University Press, 1973.

[17] James A. Franklin. *Dynamics, Control, and Flying Qualities of V/STOL Aircraft*. American Institute of Aeronautics and Astronautics (AIAA), 2002. ISBN: 978-1-56347-575-7. URL: https://app.knovel.com/hotlink/toc/id:kpDCFQVST2/dynamics-control-flying/dynamics-control-flying.

[18] ARTHUR E. BRYSON. "Attitude Control with Reaction Wheels". In: *Control of Spacecraft and Aircraft*. Princeton University Press, 1994, pp. 37–49. ISBN: 9780691087825. URL: http://www.jstor.org/stable/j.ctt17kk6rv.9 (visited on 04/14/2024).

[19] Tomáš Frank - www.propagon.cz. *80 KW electric motor*. Sept. 2022. URL: https://www.mgm-compro.com/electric-motor/80-kw-electric-motor/.

[20] *J79 (LeteckeMotory.cz) — leteckemotory.cz*. http://www.leteckemotory.cz/motory/j79/. [Accessed 28-04-2024].

[21] Peter Welander. *Understanding Derivative in PID Control | Control Engineering — controleng.com*. https://www.controleng.com/articles/understanding-derivative-in-pid-control/. 2010.